MEASUREMENTS OF DYNAMIC PROPERTIES OF MATERIALS

Volume II

EXPERIMENTAL METHODS AND TECHNIQUES

FINAL REPORT

by

D. R. Christman
W. M. Isbell
S. G. Babcock
A. R. McMillan
S. J. Green

Materials and Structures Laboratory
Manufacturing Development, General Motors Corporation
General Motors Technical Center, Warren, Michigan 48090

UNCLASSIFIED
Security Classification

DOCUMENT CONTROL DATA - R & D

(Security classification of title, body of abstract and indexing annotation must be entered when the overall report is classified)

1. ORIGINATING ACTIVITY (Corporate author): Manufacturing Development, General Motors Corporation, General Motors Tech. Center, Warren, Mich. 48090	2a. REPORT SECURITY CLASSIFICATION: UNCLASSIFIED 2b. GROUP

3. REPORT TITLE

Final Report - Measurement of Dynamic Properties of Materials
Volume II : Experimental Methods and Techniques

4. DESCRIPTIVE NOTES (Type of report and inclusive dates)

Final Report (in Six Volumes)

5. AUTHOR(S) (First name, middle initial, last name)

Douglas R. Christman, William M. Isbell, Stephen G. Babcock, Allan R. McMillan and Sidney J. Green

6. REPORT DATE	7a. TOTAL NO. OF PAGES	7b. NO. OF REFS
1971 August	74	38

8a. CONTRACT OR GRANT NO	9a. ORIGINATOR'S REPORT NUMBER(S)
DASA01-68-C-0114 b. PROJECT NO NWER XAXA c. Task & Subtask AA106 d. Work Unit 07	MSL-70-23 Vol. II 9b. OTHER REPORT NO(S) (Any other numbers that may be assigned this report) DASA - 2501-2

10. DISTRIBUTION STATEMENT

Approved for public release; distribution unlimited.

11. SUPPLEMENTARY NOTES	12. SPONSORING MILITARY ACTIVITY
	DIRECTOR Defense Atomic Support Agency Washington, D.C. 20305

13. ABSTRACT

Experimental methods and techniques for studying the dynamic response of materials are discussed. Descriptions cover uniaxial and multiaxial stress testing at strain rates up to ~~10^3~~ 1,000/sec, temperatures up to 4000°C and heating rates up to ~~10^4~~ 10,000°C/sec; measurements of elastic constants as functions of temperature (up to 300°C) and pressure (up to 10 kbars); flat-plate impact techniques for uniaxial strain testing at impact velocities up to 8 mm/μsec; hugoniot equation of state measurements with x-cut quartz gages and streak camera; wave profile studies using laser velocity interferometer, manganin gage, slanted resistance wire and magnetic wire techniques; and spall fracture studies using active (free surface velocity vs. time) and recovery (metallographic examination) methods. Where appropriate, data reduction and analysis procedures are described.

DD FORM NOV. 1473

UNCLASSIFIED
Security Classification

14. KEY WORDS	LINK A		LINK B		LINK C	
	ROLE	WT	ROLE	WT	ROLE	WT
Stress-Strain-Strain Rate						
Elastic Constants						
Equation of State						
Wave Profiles						
Dynamic Fracture						

DASA 2501-2
MSL-70-23 Vol. II
1971 August

MEASUREMENTS OF DYNAMIC PROPERTIES OF MATERIALS

Volume II

EXPERIMENTAL METHODS AND TECHNIQUES

"This work was supported by the Defense Atomic Support Agency under NWER Subtask AA 106"

FINAL REPORT

by

D. R. Christman
W. M. Isbell
S. G. Babcock
A. R. McMillan
*S. J. Green**

Materials and Structures Laboratory
Manufacturing Development, General Motors Corporation
General Motors Technical Center, Warren, Michigan 48090

* Presently with Terra Tek, Inc. 815 East 4th. South, Salt Lake City, Utah 48102

Prepared For

HEADQUARTERS
Defense Atomic Support Agency
Washington, D.C. 20305

Under Contract DASA01-68-C-0114

COPY No. 11

ABSTRACT

Experimental methods and techniques for studying the dynamic response of materials are discussed. Descriptions cover uniaxial and multiaxial stress testing at strain rates up to 10^3/sec, temperatures up to 4000°C and heating rates up to 10^4°C/sec; measurements of elastic constants as functions of temperature (up to 300°C) and pressure (up to 10 kbars); flat-plate impact techniques for uniaxial strain testing at impact velocities up to 8 mm/μsec; hugoniot equation of state measurements with x-cut quartz gages and streak camera; wave profile studies using laser velocity interferometer, manganin gage, slanted resistance wire and magnetic wire techniques; and spall fracture studies using active (free surface velocity vs. time) and recovery (metallographic examination) methods. Where appropriate, data reduction and analysis procedures are described.

FOREWORD - EXPERIMENTAL DATA VOLUMES

The prediction of reentry vehicle response to impulsive loading resulting from energy deposition has been studied extensively during the last decade. Analytical models and computer routines have been developed to assess the vulnerability of such vehicles to the initial loading phase, in which stress waves are generated and propagated through the structure, and to subsequent phases, where elastic vibration, plastic deformation and/or fracture may occur.

A Defense Atomic Support Agency (DASA) program was initiated with the objective of improving computer codes for the prediction of damage induced by X-rays (PREDIX). The PREDIX metals program has combined the efforts of several contractors under the direction of DASA. The primary contributions of each contractor can be summarized as follows:

General Motors Corporation--Measurement of material properties, including stress-strain-strain rate behavior, elastic constants, equations of state, shock wave profiles and spall fracture.

Effects Technology Inc.--Spall fracture tests and analysis (exploding foil) and underground testing.

KMS Technology Center--Constitutive modeling.

Physics International Company--Energy deposition and spall fracture studies (electron beam).

Systems, Science and Software--Energy deposition and front surface phenomena, constitutive modeling and code development, and underground testing.

TABLE OF CONTENTS

LIST OF ILLUSTRATIONS

LIST OF ILLUSTRATIONS (Continued)

LIST OF ILLUSTRATIONS (Continued)

INTRODUCTION

The measurement of dynamic properties of materials requires use of specialized and often sophisticated equipment and techniques to obtain satisfactory data under extreme ranges of test conditions. In particular, laboratory studies of material response to impulsive loads include pressures up to 5 megabars, temperatures up to 4000°C and loading times as low as 50 nanoseconds. These studies generally involve material characterization in four areas: (1) stress-strain-strain rate; (2) elastic constants; (3) equation of state and wave profile; and (4) dynamic fracture.

This report is a review of the facilities and techniques used for materials studies at the General Motors Corporation, Manufacturing Development, Materials and Structures Laboratory. The methods described have been used in support of the DASA-sponsored PREDIX program, experimental results of which are summarized in Reference 1 and given in detail in References 2 to 5. These reports include additional discussion on the application of the experimental techniques to specific materials.

SECTION I

STRESS-STRAIN-STRAIN RATE STUDIES

Current shock wave and structural response codes require information on the behavior of materials under uniaxial and multiaxial stress conditions. Code inputs include constitutive equations relating stress to strain and to strain rate. Measurements are made of uniaxial compressive stress vs. strain at various strain rates, giving yield and flow stress behavior, strain rate sensitivity and work hardening characteristics. The measurements are sometimes extended to uniaxial tension, and testing in orthogonal directions is necessary if material anisotropy is significant. Bauschinger effect tests provide information on unloading and subsequent yield. Because of the temperature increase normally associated with energy-deposition loading, it is important to establish the influence of material temperature as well as heating rate and time-at-temperature on strength properties and stiffness. Finally, extension of calculations to include long-time structural response requires information on yield and fracture surfaces for multiaxial stress states.

UNIAXIAL STRESS TESTS

Low Rate Testing

Uniaxial stress testing at low rates (<0.1/sec) is done on an Instron Model TT-D Universal Testing Instrument with load

capacity of 20,000 lbs. Tension and compression tests are carried out at temperatures from -195°C to +500°C, with load-strain recorded on an X-Y recorder.

Medium Rate Testing[6-8]

Medium strain rate testing is carried out at 10^{-3}/sec to 10^{2}/sec using the gas-operated medium-strain-rate machine shown in Figure 1. The machine is capable of either upward or downward piston motion for compression or tension testing, respectively. The maximum strain rate depends on accuracy required and on specimen material and geometry since stress waves generated by high velocity motion can impede accurate time resolution of stress and strain in the specimen. The upper limit is generally between 30 and 100/second. The load applied to the specimen is measured by strain gages mounted on an elastic load bar directly above the specimen. Specimen strain is obtained by measuring piston displacement, by use of an optical extensometer, or by using strain gages.

The optical extensometer used is a Physitech Model 309 with dual tracking units. This device will detect a discontinuity in light intensity, such as the edge of a black and white band on a specimen, and gives a voltage output proportional to the position of the edge as the specimen is strained. To operate the extensometer, the test specimen is marked with paint as shown in Figure 2. One tracker is focused on the upper portion of the gage length and the other on the lower portion. The extensometer is set so that the difference between movement of the upper and lower portions of the test specimen is recorded as output. This difference, divided by the original distance between the two marks, is the engineering strain.

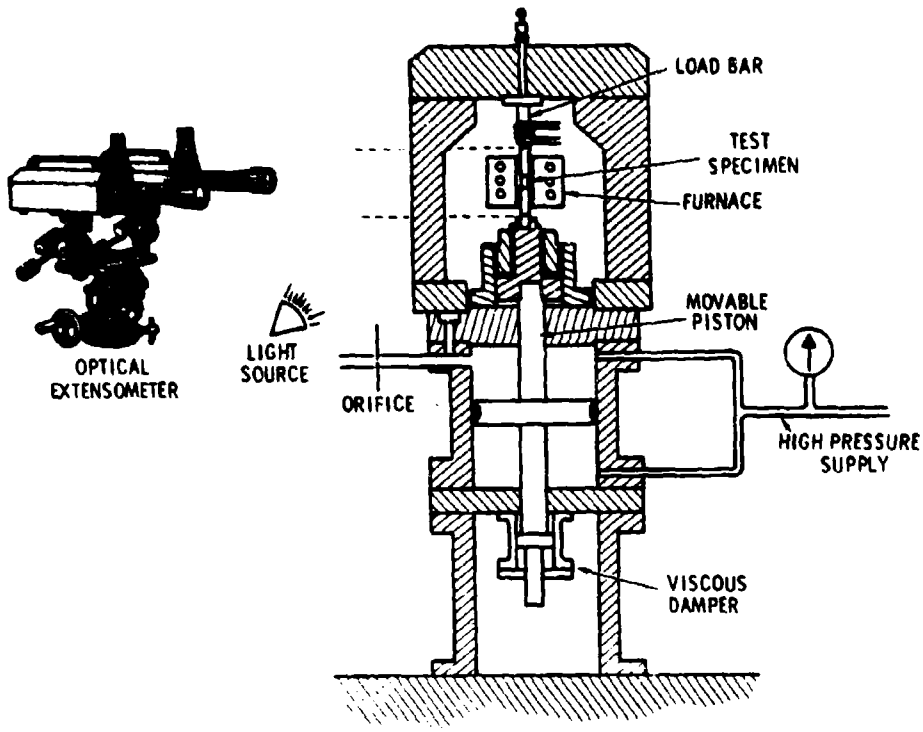

Figure 1 Medium-Strain-Rate Machine Schematic

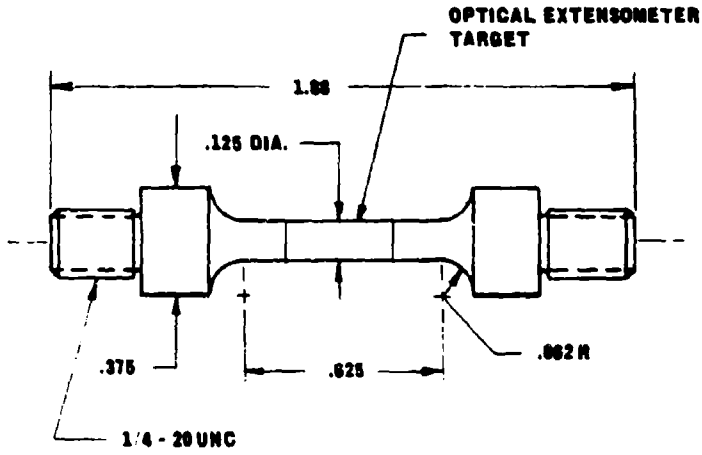

Figure 2 Tension Specimen for Medium-Rate Machine

For testing at temperatures up to 500°C, a Research Incorporated Model ZH3A furnace is used. This furnace is divided into three independently-controlled zones containing tungsten-filament quartz heating elements. A water-cooled heat exchanger is attached to the load bar to isolate the strain gages from the furnace heat. Specimen temperature is monitored with thermocouples placed in contact with each end of the specimen. These thermocouples are used to control the heating elements through the furnace controller. Specimens can be heated at a selected constant heating rate and held at a given temperature for as long as desired.

High Rate Testing[8-11]

High strain rate tests from about 2×10^2 to 5×10^3/sec are conducted on a Hopkinson bar device. The operation of the Hopkinson bar is based upon the theory of one-dimensional elastic wave propagation. Using this theory, deformation of a specimen sandwiched between two elastic bars and subjected to a stress wave may be calculated. Compression or tension tests can be carried out, as shown in Figures 3 and 4. The specimen behavior is obtained by measuring the output from strain gages mounted on the load bars on both sides of the specimen and applying one-dimensional elastic wave theory. The problem of nonuniformity of axial stress (axial inertia) in the early stages of testing (typically 1 to 2% strain at 10^3/sec), where the specimen is being loaded by wave reverberations, makes interpretation of yield stress difficult. Also, the major assumption of uniaxial stress in the early stages will not be valid if radial inertia effects have not been eliminated. These effects are present immediately behind the wave front where radial, or transverse, stress waves propagate to the specimen sides and reflect back. Until these waves have reflected

several times, a nonuniform stress distribution exists. This limits the upper strain rates achievable to a few thousand per second, since for higher strain rates the entire test (to 10-15% strain) will occur in the nonuniform stress condition. The calculation of the stresses beyond yield is estimated to be accurate to about 10%, although reproducibity is much better.

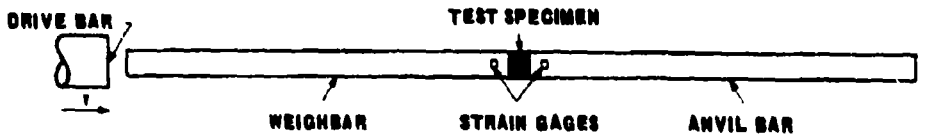

Figure 3 Compression Device for Hopkinson Bar

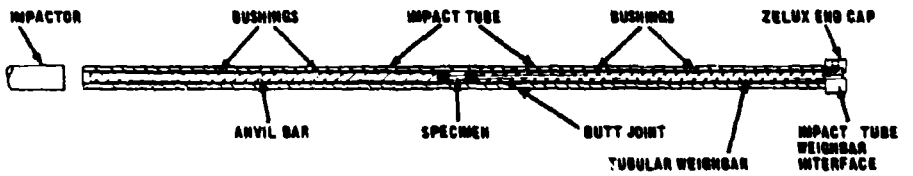

Figure 4 Tension Device for Hopkinson Bar

Elevated temperature testing with the Hopkinson bar is done in compression only, and the technique is shown in Figure 5. The specimen is heated in a radiant-heat furnace similar to that used on the medium rate machine. The specimen is brought up to temperature with the load bars isolated outside the furnace. At test temperature, a pneumatically-operated device quickly moves the bars into contact with the specimen and triggers the acceleration of the driver bar down the launch tube to impact the weigh-bar. This procedure eliminates any significant temperature increase in the bars at a distance of

1 mm from the specimen/bar interface for about 3 seconds, much longer than the time for the stress wave to be initiated and the 160 μsec stress pulse to propagate through the specimen.

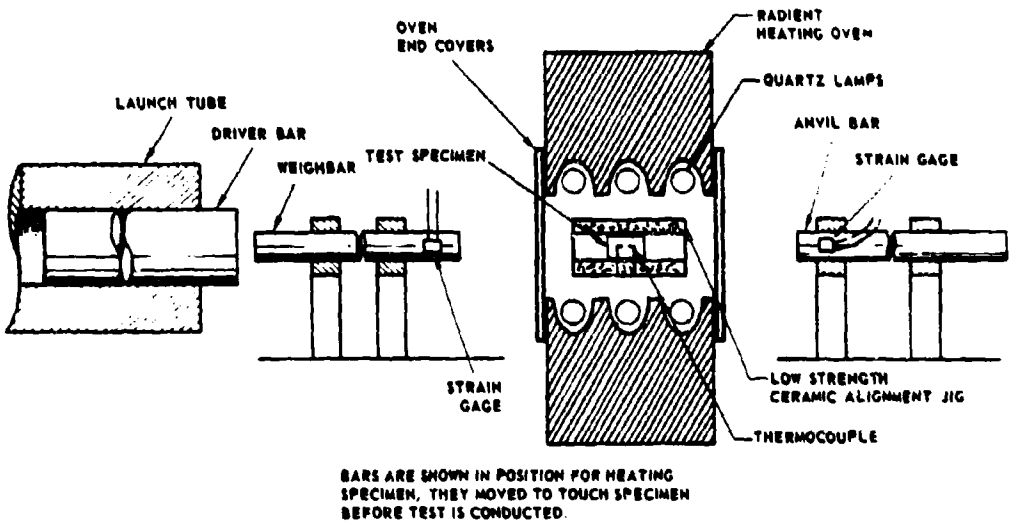

Figure 5 Elevated Temperature Technique for Hopkinson Bar

Data Reduction

Data from the medium and high rate tests is obtained in analog form on film. The records are digitized on a telereader and a computer program is utilized to obtain stress, strain and strain rate vs. time. Appropriate calibration factors are incorporated, including oscilloscope gain, machine stretch and stress bar behavior. Plot routines are used with a Cal-Comp Model 565 Plotter to present results in graphical form for analysis.

MULTIAXIAL STRESS TESTS

Biaxial Machine[12,13]

This machine, shown in Figure 6 and 7, develops a biaxial state of stress by applying an axial load and a circumferential load simultaneously. The loads are applied on a tubular specimen through two independent gas-operated cylinders. The axial stress can be tension or compression, while application of internal or external pressure gives circumferential tension or compression. Axial and/or circumferential strain rates from 10^{-3} to about 10/sec are possible. Three dimensional yield and/or fracture surfaces can be mapped at various strain rates and constitutive equations relating stress, strain and strain rate can be derived for multiaxial stress deformation states.

Confined Pressure Device[14]

For confined pressure testing, a pressure chamber replaces the standard compression specimen package, and can accomodate both tubular and solid cylindrical specimens. The machine frame is used to equalize the hydrostatic component of the axial load so that the driving cylinder must overcome only the material reaction to deformation. The axial load is measured by a strain-gaged load cell mounted inside the pressure vessel to eliminate friction load from the seals. Pressure is measured with diaphragm-type pressure transducers. Axial and tangential specimen strains are obtained from strain gages mounted on the specimen.

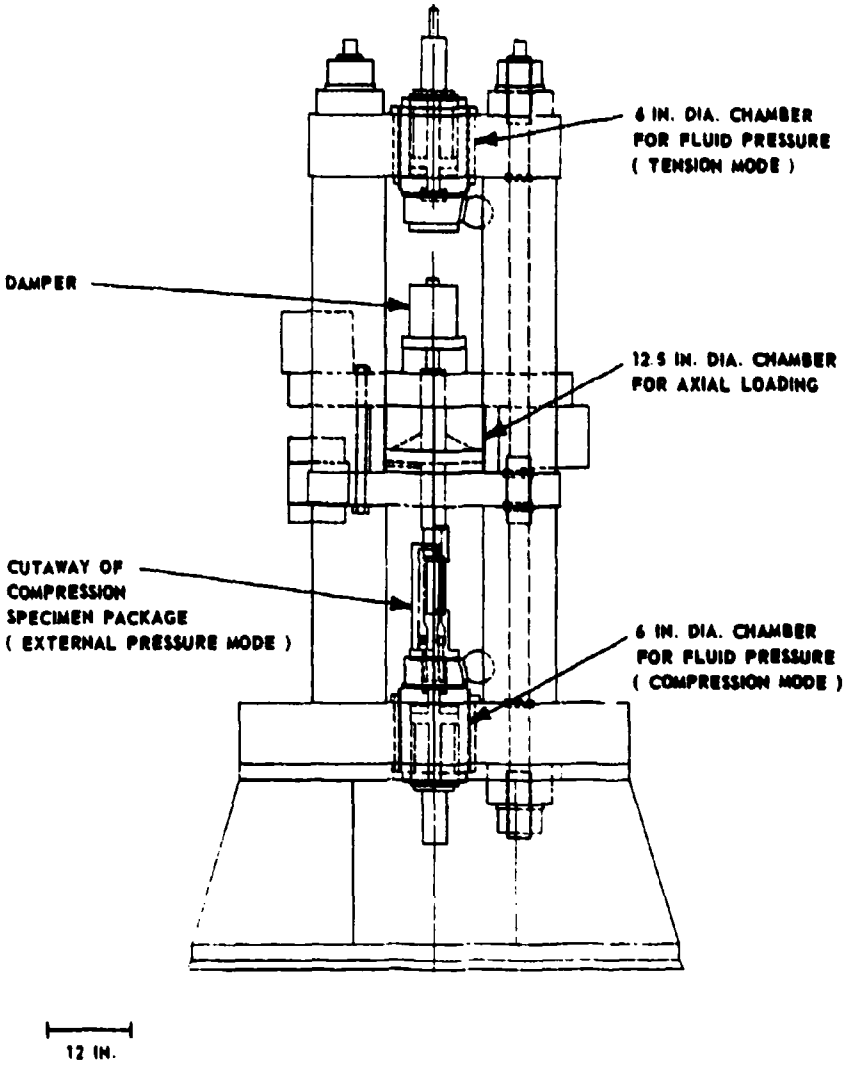

Figure 6 Biaxial Medium-Strain-Rate Machine Schematic

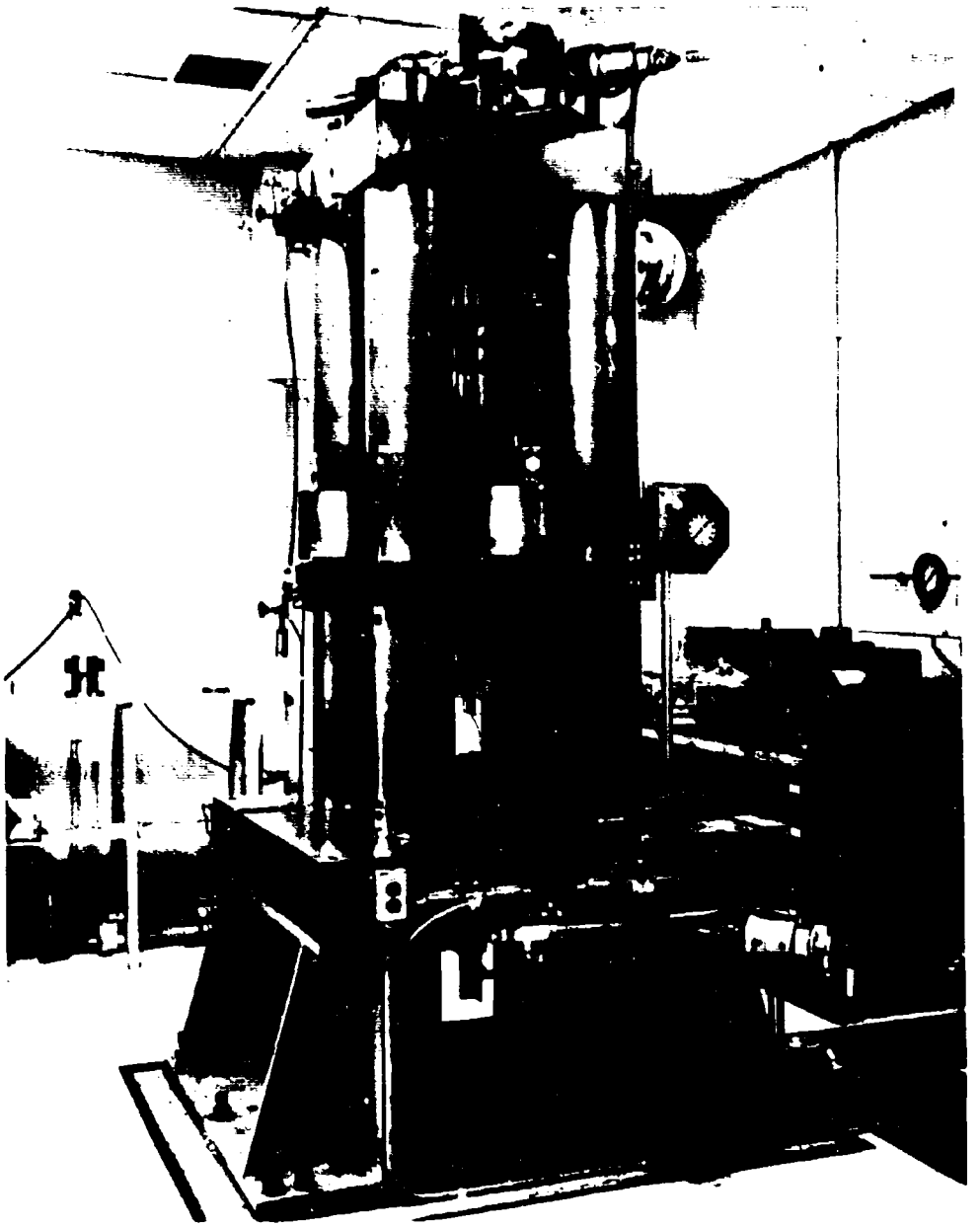

Figure 7 Biaxial Medium-Strain-Rate Machine

Data Reduction[15]

Data recording is done with a Consolidated Electrodynamic Corporation fourteen-channel, 400KHz-bandpass FM tape recorder. The reduction of fourteen channels of data to a computer-compatible form is achieved by direct analog-to-digital (A/D) conversion from the tape system. This technique omits intermediate steps (recording data on film, manual digitizing of data, etc.) thereby reducing cumulative error as well as retaining the analog data for future reference. The A/D converter is interfaced to an IBM 1800 Central Processor. This system has the capability to digitize, store the data in digital form and input the proper scale and calibration factors. A plotter and a low-speed line printer are used as primary data output devices.

HIGH HEATING RATE TESTS[16,17]

Heating and Testing Machine

Electrically conductive materials can be tested at high heating rates and medium strain rates on a modified medium-strain-rate machine. Direct resistance (I^2R) heating at rates up to 10^4°C/sec and temperatures up to 4000°C is used to study the high heating rate properties of materials. Figures 8 and 9 show the device. Load is measured with semiconductor strain gages mounted on the water-cooled elastic load bar directly above the specimen. A plug-in strain gage monitor is used to record load and specimen displacement as a function of time. Through an electronic switching panel, either uniaxial load or bending load in two orthogonal directions can be measured.

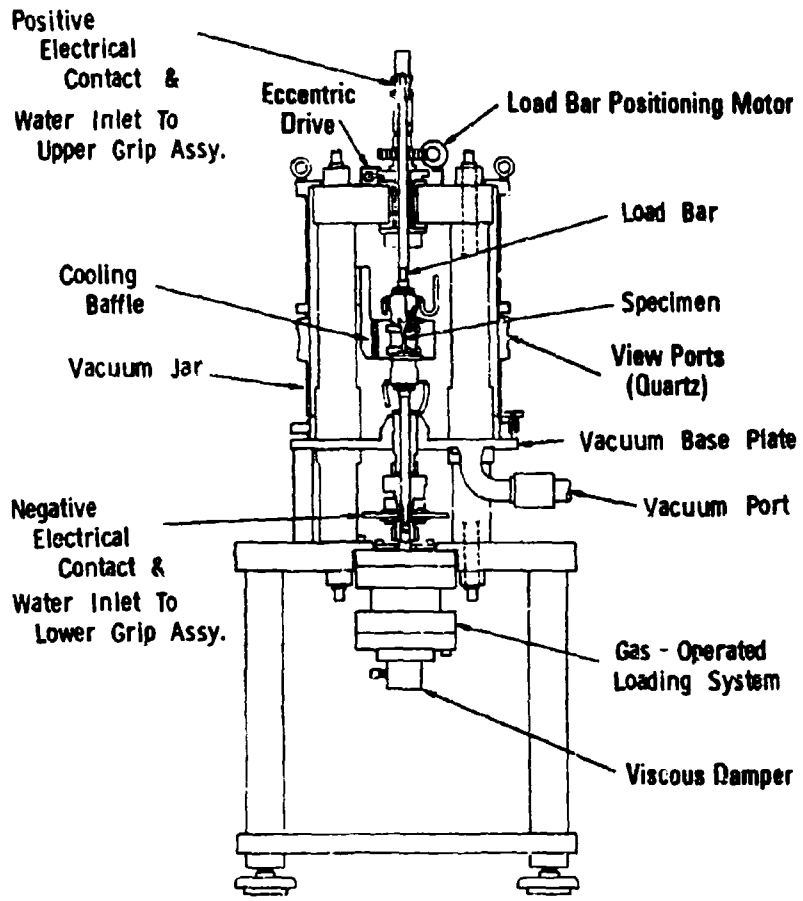

Figure 8 High-Temperature Medium-Strain-Rate Machine Schematic

Heating is accomplished with a direct resistance method. An 800 amp, 50 volt regulated direct-current power supply, capable of 1200 amp outputs for periods up to one second, is connected to the test sample through copper electrodes. Specimen grip design allows temperature extremes up to 4000°C on graphite materials while maintaining moderate temperatures (below 800°C) in the grip jaws and load bars. To reach temperatures above 2800°C specimen radiation losses must be minimized. This is

done by surrounding the specimen-grip area with a cast alumina and boron nitride shield into which a graphite felt and pyrolytic graphite liner is placed. Two small holes accomodate material outgassing and optical viewing of the specimen. To achieve precise and repeatable heating profiles from test to test, the power supply is coupled to a high-speed temperature controller, and predetermined heating rates and time-at-temperature can be programmed.

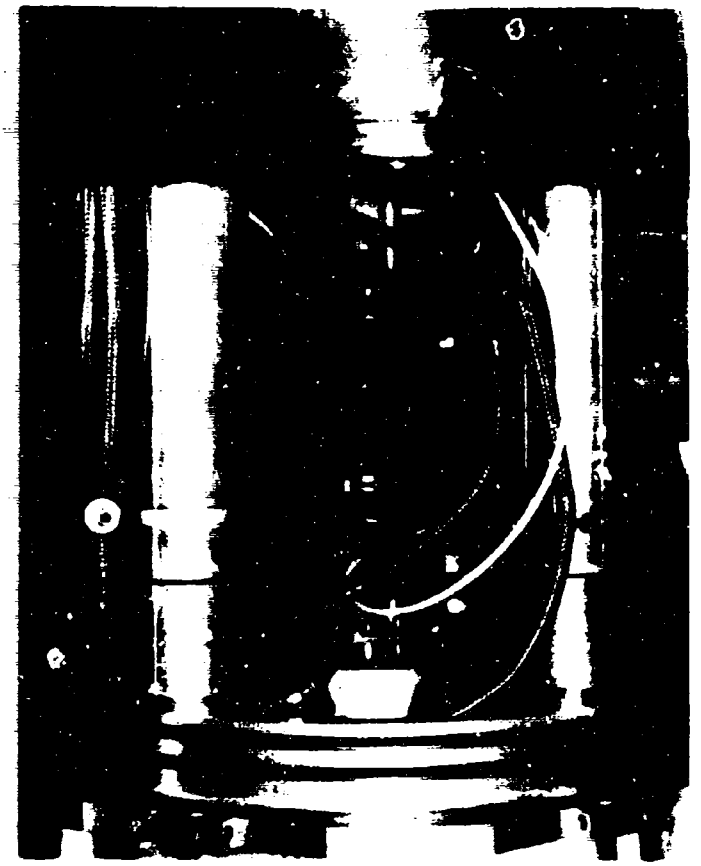

Figure 9 High-Temperature Medium-Strain-Rate Machine Test Chamber

Temperature Measurement

Inherent in heating and testing materials at high temperatures is the uncertainty in the determination of the material temperature. The technique used with the high-temperature medium-strain-rate machine utilizes pyrometry, temperature measurement of hot bodies using self-emitted radiation. Optical pyrometers are used to measure temperature in the range of 20° to 4000°C. A Barnes Engineering Co. Model RM2A Radiometric Microscope is used for temperatures from 20° to 1000°C, while a Pyrometer Instrument Co., Model A144 Automatic Optical Pyrometer is used in the range 800° to 4000°C. Both units have response times fast enough to measure temperature changes near $5X10^{3}$°C/sec and are calibrated for emissivity corrections.

Strain Measurement

Conventional strain measuring techniques such as strain gages or mechanical extensometers suffer severe drawbacks when used at high temperature or high loading rates. Even the most sophisticated commercially-available optical tracking systems are inadequate at temperatures where gage marks will not adhere to the sample or radiant glow from the specimen interfers with the tracker response. To circumvent these problems, an optical strain measuring technique was developed to measures small dynamic strains at temperatures up to 4000°C.

An argon CW laser (4880Å) scans the sample surface through a quartz window and is reflected onto a photomultiplier tube as shown in Figure 10. By operating at this wavelength, radiant energy from the surface of the hot sample does not interfere with the laser signal. A telescope then transfers the image

of the laser-illuminated gage section to the narrow-band PM tube. Electronic processing of this signal results in determination of gage section displacement (and hence specimen strain) as a function of time. Laser scanning of the surface at approximately 40 KHz is provided through an acoustic-optic diffraction cell. Strains as low as 10^{-4} occuring in times of one millisecond or longer can be measured. Specimen gage sections consist of RF-sputtered thin films of refractory metals such as tantalum, molybednum or hafnium deposited in thicknesses of approximately one micron.

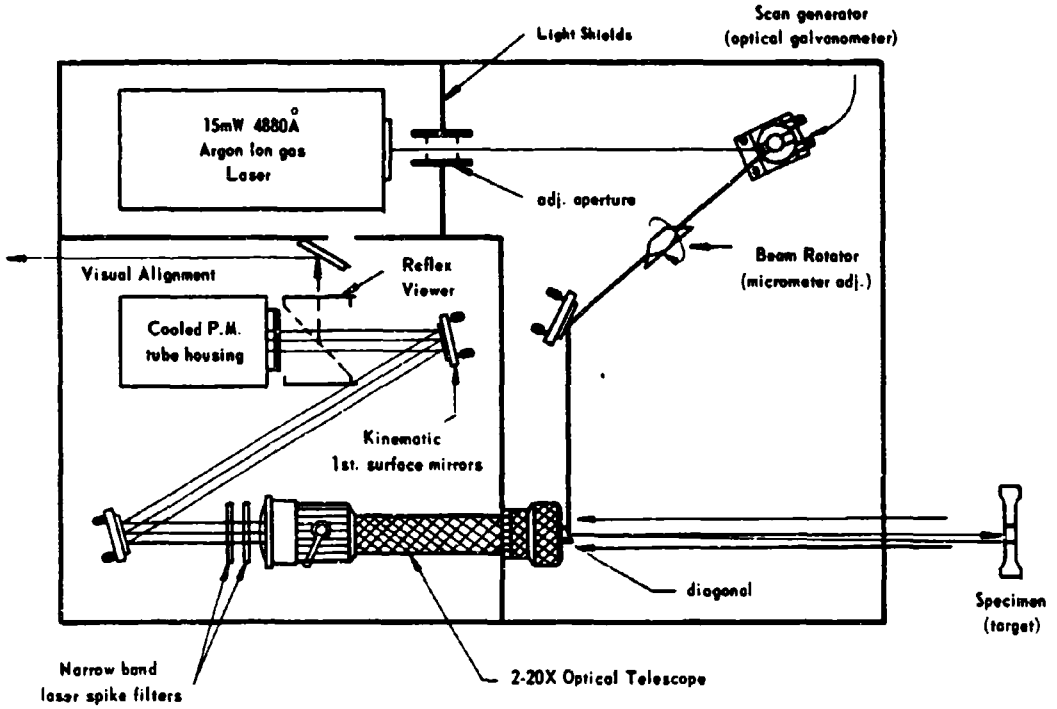

Figure 1.0 Scanning Laser Extensometer Schematic

SECTION II

ULTRASONICS MEASUREMENTS

Measurement of elastic constants of materials provides necessary inputs to the study of material response. Three basic measurements are density (ρ), longitudinal wave velocity (C_L) and shear wave velocity (C_S). Ultrasonics measurements of wave velocities at standard temperature and pressure (i.e., 20°C and atmospheric pressure) establish the parameters used in first-order (temperature and pressure independent) calculations of dynamic material behavior. Measurement of the temperature and pressure dependence of the wave velocities permits more exact calculations to be made and, in particular, leads to prediction of pressure-compression isotherms, adiabats and hydrostats. If the temperature and pressure dependence is measured with sufficient accuracy ($\leq$0.1%), the calculated pressure-compression behavior can frequently be extrapolated with reasonable confidence to higher pressures than covered in the actual measurements.

ELASTIC WAVE VELOCITIES

Pulse Superposition[18,19]

Pulse superposition techniques give high accuracy ($\sim$0.02%) for velocity measurements, and offer ease of measuring a change in velocity due to a change in temperature or pressure. The technique is shown schematically in Figure 11. A transducer, of

either longitudinal or shear mode, is bonded to one end of a specimen with parallel, flat faces. A short radio frequency (RF) burst, matched in frequency to the resonant frequency of the transducer, is applied. The transducer, which is both a transmitter and receiver, transmits an ultrasonic wave into the specimen. This wave reflects off the back surface of the specimen and is received as an echo by the transducer. If a second RF burst is applied at the exact time this first echo is received, etc., the echo amplitudes will superpose. In order to determine when exact superposition occurs, the RF bursts are interrupted and the decaying echos are observed. The repetition rate of the RF bursts, which determines the time between pulses, is adjusted to give maximum echo amplitudes, i.e., exact superposition. The wave transit time through the specimen is then one-half the reciprocal of the oscillator frequency controling the RF repetition rate.

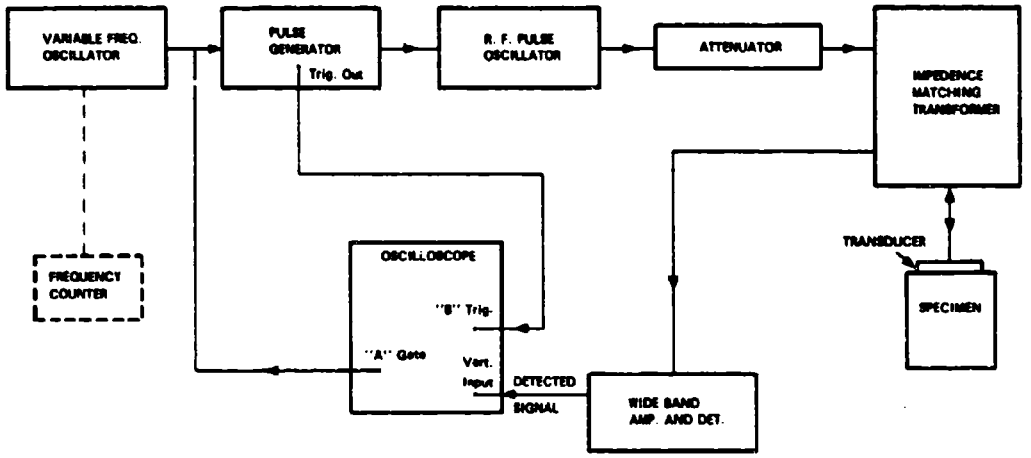

Figure 11 Pulse Superposition Technique Schematic

Pulse Transmission[19,20]

The pulse transmission technique is used when attenuation of RF pulses is too high to give sufficient measurable echoes in the pulse superposition mode. The accuracy is somewhat less (∿0.05%) than pulse superposition. The technique is shown schematically in Figure 12. A pulse is applied to the transmitting transducer, passed through the specimen and received at the transducer on the opposite face, delayed by the transit time through the specimen. A comparison pulse is matched to the shape of the received pulse and is in turn used to adjust the shape of the initial pulse. Once the initial, delayed and comparison pulses have the same shape, the oscillator frequency is adjusted to obtain an exact multiple of comparison pulses between the initial and delayed pulses. The reciprocal of the oscillator frequency times the number of comparison pulses equals the transit time through the specimen.

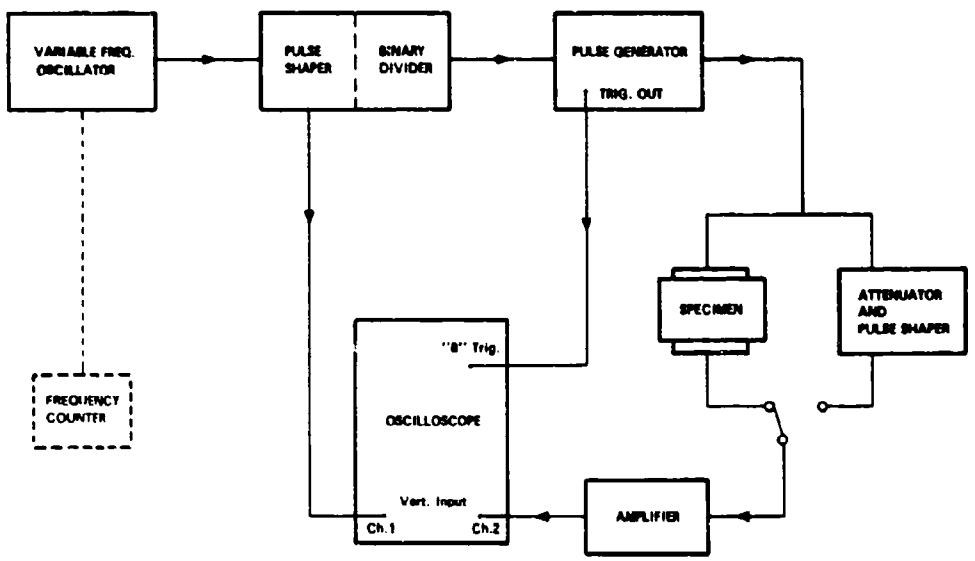

Figure 12 Pulse Transmission Technique Schematic

Temperature and Pressure Dependence[21,22]

The temperature dependence of elastic wave velocities is determined by immersing the specimen and transducer in a constant temperature bath. Generally, the upper temperature limit is determined by the transducer/specimen bond material and is about 300°C for longitudinal waves and 100°C for shear waves. Both pulse superposition and pulse transmission methods can be used. Specimen length must be corrected for thermal expansion to obtain correct velocities.

The static high-pressure apparatus is shown in Figure 13 and employs a Harwood Engineering Co. pressure intensifier system.

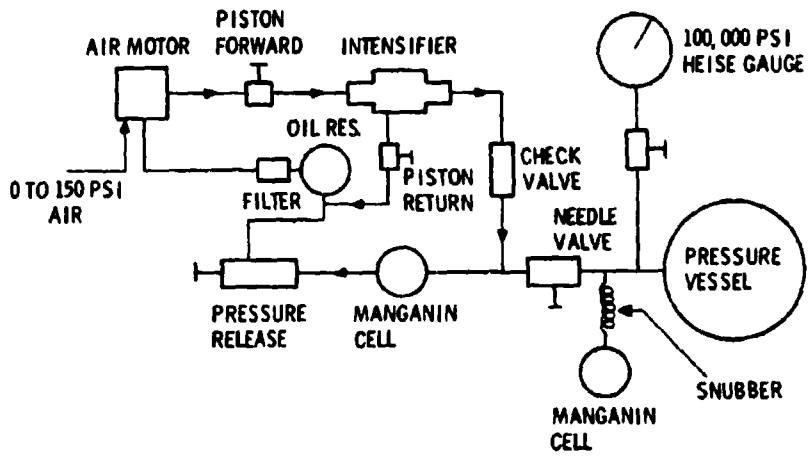

Figure 13 Static High-Pressure Apparatus Schematic

The hydraulic system consists of two parts: a low-pressure portion which transmits pressure to the large piston in the intensifier, and a high-pressure portion which transmits pressure to the pressure vessel containing the specimen. The usable portion of the pressure vessel is 2.5cm diameter by 15cm long and the

pressure range is 0-9 kbar. Since pressure dependence is determined under isothermal conditions, temperature of the working fluid is monitored. Both pulse superposition and pulse transmission methods are used, with the specimen length corrected for hydrostatic compression to obtain correct velocities.

ELASTIC CONSTANTS[23-25]

Once the longitudinal and shear wave velocities have been determined, the elastic constants can be calculated. Assuming the material is isotropic, the adiabatic elastic constants at 20°C and zero pressure are obtained as follows:

$$\nu = [0.5-(C_S/C_L)^2]/[1.0-(C_S/C_L)^2]$$

(Poisson's Ratio)

$$C_B = \sqrt{C_L^2-4/3\ C_S^2}$$

(Bulk Wave Velocity)

$$C_E = \sqrt{2(1+\nu)\ C_S^2}$$

(Sound wave velocity, longitudinal wave of infinite wave length in bar, lateral displacement allowed.)

$$C_R:\quad k_1^6 - 8k_1^4 + (24-16\alpha_1^2)k_1^2 + (16\alpha_1^2-16) = 0$$

where $k_1^2 = (C_R/C_S)^2$, $\alpha_1^2 = (C_S/C_L)^2$

(Rayleigh or Surface Wave Velocity)

$$K = \rho C_B^2 = \rho (C_L^2 - 4/3 C_S^2)$$

(Bulk Modulus)

$$G = \rho C_S^2$$

(Shear or Rigidity Modulus)

$$E = 2\rho(1+\nu)\, C_S^2$$

(Young's or Elastic Modulus)

$$\lambda = 2\rho\nu C_S^2/(1-2\nu)$$

(Lamé's Parameter)

After C_L and C_S are measured as functions of temperature (T) and pressure (P), the data are corrected for thermal expansion and hydrostatic compression. The adiabatic bulk and shear modulii (K and G) can then be determined as functions of T and P, after correcting for change in density. Finally, for use in compressibility calculations, the isothermal values of K and G and the adiabatic and isothermal pressure derivatives are evaluated at ambient conditions (i.e., 20°C and zero pressure).

SECTION III

EQUATION OF STATE AND WAVE PROFILE STUDIES

The development of models of dynamic material behavior and the calculational codes used in predicting material response requires extensive data on material properties under uniaxial strain conditions, including hugoniot equation of state, wave propagation and spall fracture. Most data are used directly in developing models of material behavior, although independent check data (e.g., attenuated wave shapes and spall fracture profiles) are necessary to determine accuracy of the calculations.

The hugoniot is the locus of equilibrium states reached after shocking of a material. Data are usually obtained either as stress-particle velocity points from x-cut quartz gages or as shock velocity-particle velocity points from optical techniques, and may be expressed in several forms. A convenient form for experimental work is the hugoniot centered about zero stress and particle velocity, as established by a least-squares fit to the data in the stress-particle velocity (σ-u_p) plane. Transformation of the hugoniot into various planes, such as shock velocity-particle velocity (U_s-u_p) and stress-volume (σ-v), is performed by the assumption of a material model. Frequently, an ideal elastic-plastic wave structure with equilibrium initial and final states is applied to the mass and momentum conservation equations. This leads to:

$$\sigma_H = \sigma_{HEL} + \rho_e (U_s - u_e)(u_p - u_e)$$

$$v = v_o \left(1 - \frac{u_e}{C_L}\right)\left(\frac{U_s - u_p}{U_s - u_e}\right)$$

where σ_{HEL} is hugoniot elastic limit, v is specific volume and ρ_e and u_e are density and particle velocity at the elastic limit.

Therefore, when either σ_H-u_p or U_s-u_p relations are established experimentally and σ_{HEL}, ρ_e, u_e and C_L are known, σ_H, U_s, u_p and v are uniquely determined.

Profiles of shock waves propagated through a specimen are obtained as stress-time or velocity-time histories. Profiles may be used in this form directly for comparison with calculated or predicted material response. When it is necessary to transform the data to obtain material stress, particle velocity or strain (an example is the study of compressive wave development and elastic precursor decay), an impedance matching technique is applied, utilizing the conservation relations and assuming time-independent behavior. For wave systems showing time-dependency, wave loading and unloading behavior is studied by analysis of constant stress or constant particle velocity characteristics is the x-t plane.

GAS GUNS[26,27]

Gun-launched, flat-plate impact techniques are used for generating uniaxial strain conditions required for equations of state and wave propagation studies. Gun techniques give close control over stress-time history of the input pulse, permit change in the shape of the pulse, are compatible with the use of high-resolution diagnostic techniques, and facilitate recovery of specimens for post-impact analysis.

Compressed-Gas Gun, 102mm

A 102mm, single-stage, compressed-gas gun is used to launch stress-free flat plates at velocities up to 0.6mm/μsecond. The gun is shown in Figures 14 and 15. The piston head is seated by filling the rear chamber with about 80 psi air and the high pressure chamber is filled to the desired firing pressure. The gun is fired by releasing the air from the rear chamber and then rapidly introducing air into the firing chamber. The piston is forced to the rear and the high-pressure gas drives the projectile down the barrel. Air is supplied from a three-stage, high-pressure air compressor for velocities less than 0.4mm/μsec, while bottled helium is used for higher velocities.

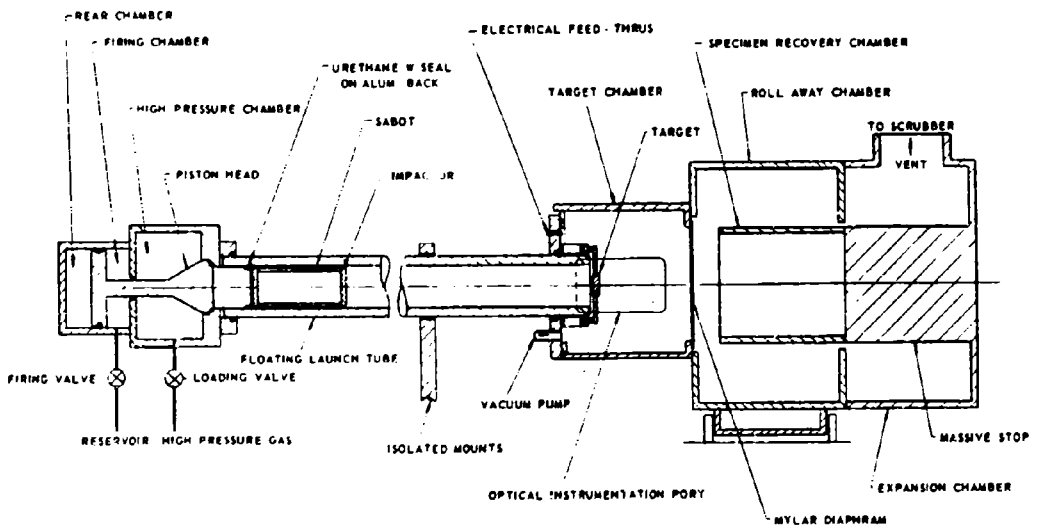

Figure 14 102mm Compressed Gas Gun Schematic

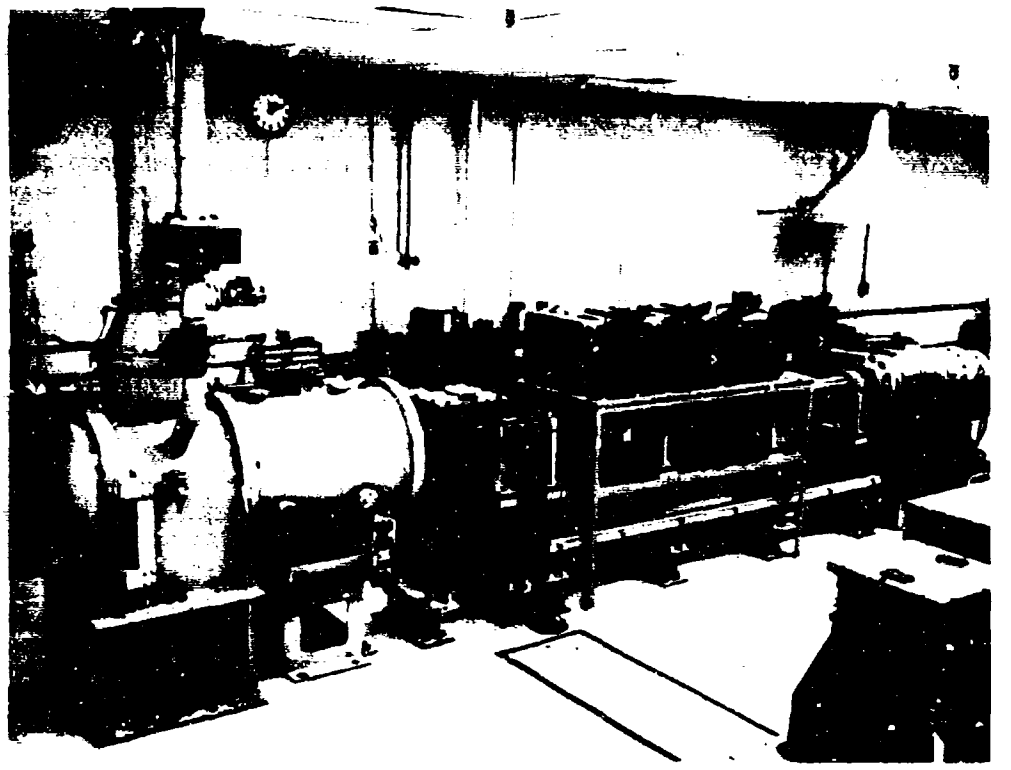

Figure 15 102mm Compressed Gas Gun

The projectile used in the 102mm gun has three basic parts: a micarta sabot; a flat plate (impactor) bonded to the front of the sabot; and a flexible, polyurethane seal bonded to the rear of the sabot to prevent blow-by of the compressed gas. The effect of air build-up between the impactor and target is minimized by evacuating the barrel and target chamber prior to firing, and by providing an expansion chamber between the end of the barrel and the target assembly. The target is shock-mounted to prevent premature motion before impact, and additional shock isolation is provided by mounting the high pressure chamber and the impact chamber on separate concrete pads.

Special attention is given to achieving a planar impact. Impacting surfaces are generally lapped flat to less than 0.5μm over the region of interest. Before firing, the target is aligned with the projectile in the angular position it will have at impact. Planarity of impact is measured with tilt pins and is generally less than $\sim 10^{-4}$ radians. Impact velocity is measured to better than ±0.2% with a shorting pin system in which charged wires are placed between the end of the launch tube and the target. These pins are at accurately measured locations along the flight line of the projectile. Upon being struck by the impactor support plate (which is grounded), each pin is shorted and the resultant signal stops a counter with 10nsec time resolution.

Compressed-Gas Gun, 63.5mm

The 63.5mm gun, shown in Figures 16 and 17, is used for launching smaller projectiles at velocities up to 0.5mm/μsecond. The test chamber instrumentation consists of a velocity measurement system and a single-flash photography station. The velocity system includes a light source, a collimating lens, and five sets of equally spaced slits in the launch tube. These slits create five narrow, parallel light beams crossing the launch tube and emerging from holes on the opposite side, where they are focused by another lens onto the sensitive element of a photomultiplier tube. An opaque projectile passing through the launch tube successively interrupts these light beams, so that when the output of the photomultiplier is recorded with an oscilloscope, projectile velocity can be measured to within ±1%.

This gun is used primarily for spall testing, and projectile/target alignment methods as well as elevated temperature techniques are described below in the section on spall tests.

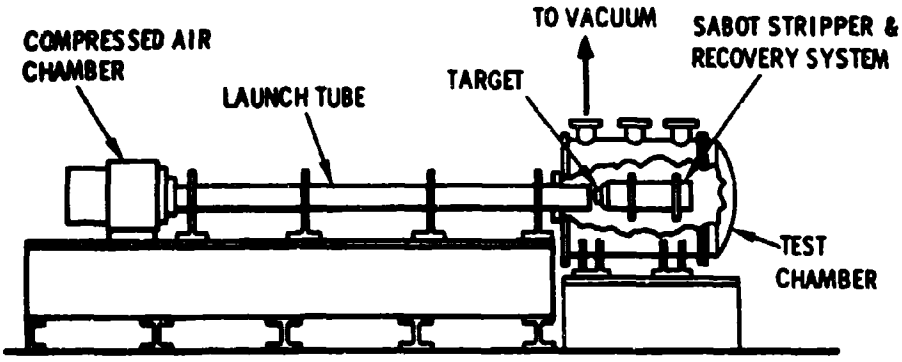

Figure 16 63.5mm Compressed Gas Gun Schematic

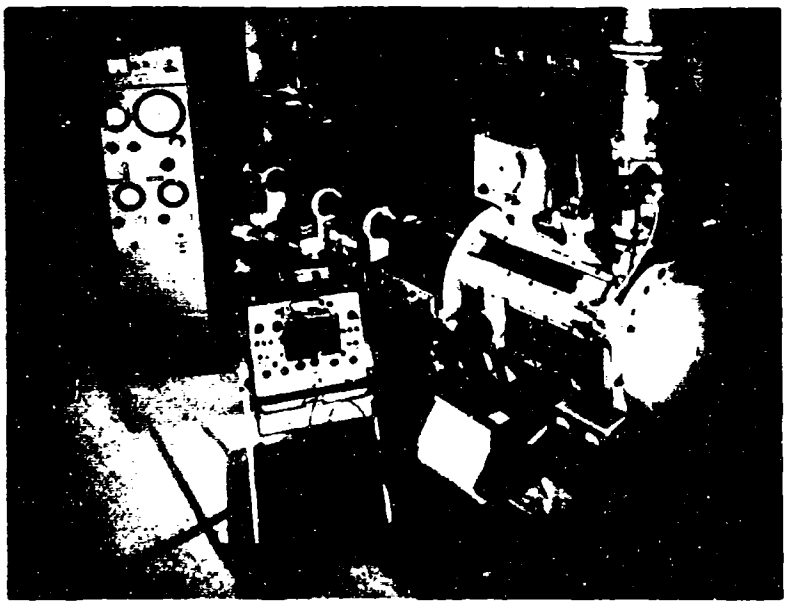

Figure 17 63.5mm Compressed Gas Gun

Light-Gas Gun

An accelerated-reservoir light-gas (ARLG) gun is used for velocities in the range of 0.6 to 8mm/μsecond. Launch tube diameters are 29mm and 64mm (3mm/μsec max. velocity for the larger launch tube). An ARLG gun maintains a reasonably constant pressure on the base of the projectile during launch, allowing a relatively gentle acceleration with negligible heating. The gun is shown in Figures 18 and 19 and operates as follows:

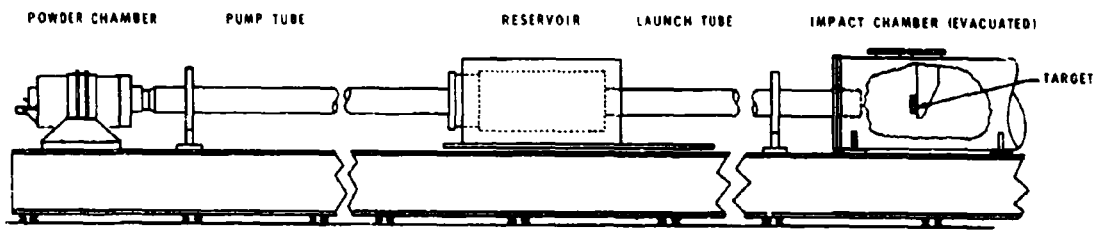

Figure 18 Accelerated-Reservoir Light-Gas Gun Schematic

A. A weighted, plastic-nosed piston is placed in the pump tube breech and the projectile is placed in the launch tube breech.

B. Gunpowder is loaded into the powder chamber and the pump tube is filled with hydrogen.

C. The gunpowder is ignited, propelling the piston down the pump tube, which compresses the hydrogen.

D. A high-pressure, burst diaphragm ruptures, letting the expanding hydrogen accelerate

the projectile down the launch tube. The piston is stopped in a tapered section between the pump tube and the launch tube.

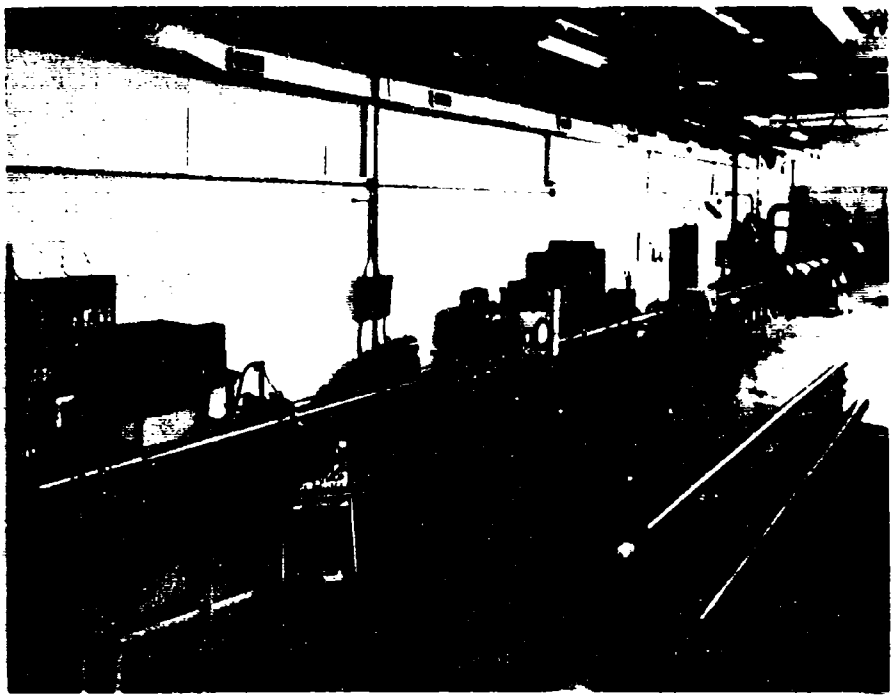

Figure 19 Accelerated-Reservoir Light-Gas Gun

Prior to firing, the launch tube and target chamber are evacuated and then flushed with helium to $\sim 10^{-2}$ torr to eliminate effects of gas build-up and ionization between projectile and target. A plastic sabot is used to hold the projectile, and the rear of the sabot has sealing lips which are pressed against the inside of the launch tube by an interference fit to prevent

blow-by of high pressure gas. The ARLG gun can be modified by putting the powder chamber at the breech end of the launch tube, giving a single-stage gun. This permits launch velocities of 0.3 to 1.5mm/μsec for projectiles up to 64mm diameter.

The instrumentation chamber is shown in Figures 20 and 21. The launch tube is inserted into the chamber through an O-ring seal, and the chamber is shock-mounted to prevent target displacement before impact. Several ports are available for optical, X-ray and instrumentation access. The impact velocity measuring system consists of a two-channel laser triggering system and short-duration (30nsec) flash X-ray pulsers. This system gives accuracy in velocity measurement of better than 0.05%. Pictures taken with the flash X-ray also show projectile tilt and integrity.

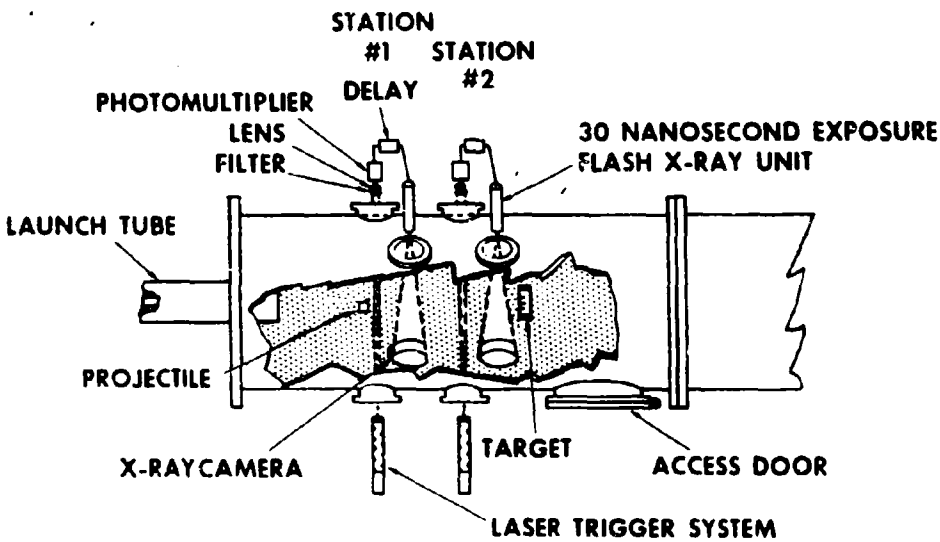

Figure 20 Target Chamber Detail, ARLG Gun

Figure 21 Target Chamber, ARLG Gun

The control room for remote loading and firing of the ARLG and 102mm guns is shown in Figure 22. The equipment shown includes an X-Y recorder for monitoring temperature vs. time; the control console for the flash X-ray system; 10-nsec time-interval counters; gas loading and gun fire-control panel; streak camera remote control unit; and 1-nsec time-interval counters.

INSTRUMENTATION

X-Cut Quartz Gages[28]

X-cut quartz crystals generate a current when opposing faces are at different stress levels. In shock wave applications, one face remains at zero stress while the face in contact with the specimen is subjected to a time-varying stress pulse. Measure-

ment of the generated current as a function of time permits calculation of stress-time history. The quartz gage is generally used in two configurations: direct impact or transmitted wave.

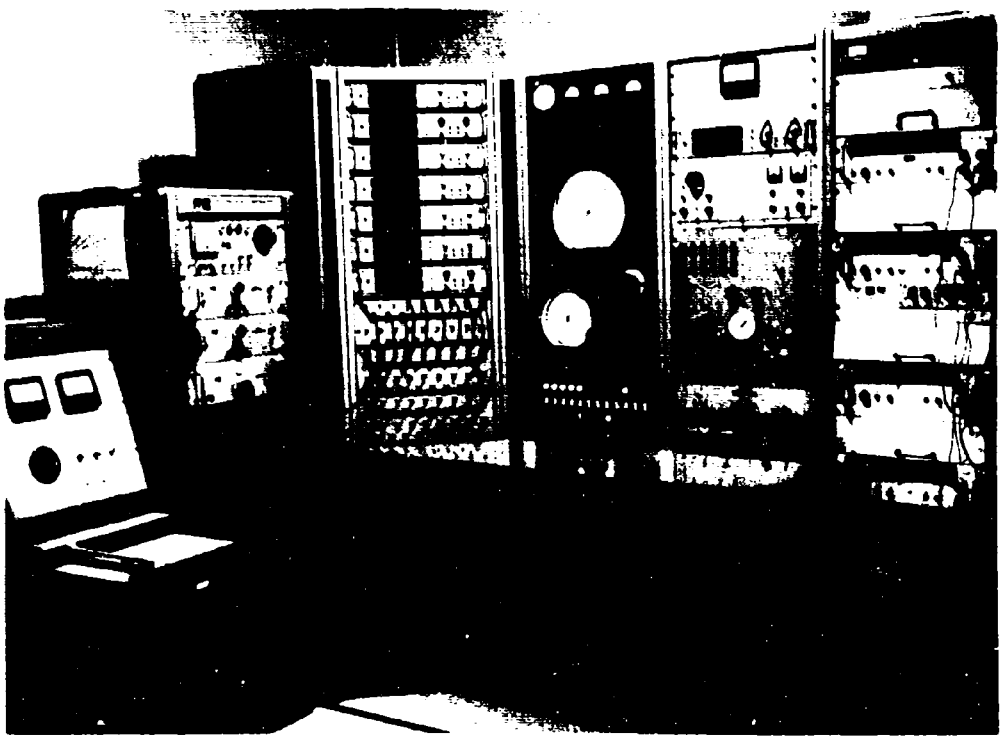

Figure 22 Control Room

Direct Impact

The direct impact technique is shown in Figure 23. At impact, one stress wave propagates into the quartz crystal and one into the impactor or specimen. The current generated by the stress difference between the impact face and the rear face of the

quartz is collected from an electrode in the center of the rear face of the crystal, with the impact face at ground potential. The current is passed through low-loss, foam-dielectric cable to Tektronix 547 and 454 oscilloscopes, and the piezoelectric current vs. time signal is recorded on film. Current and time calibration traces are recorded on the same record.

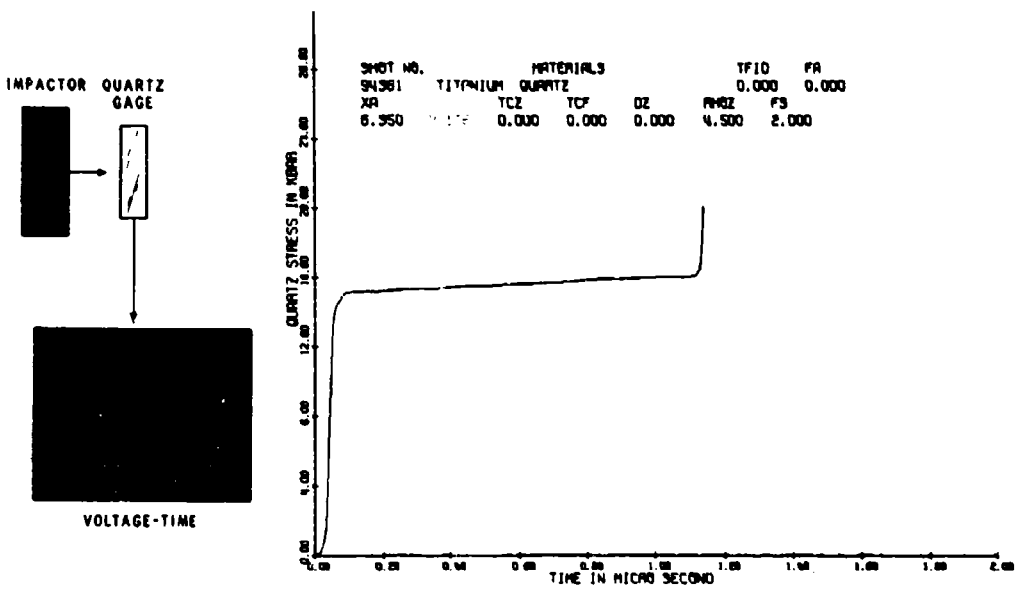

Figure 23 Quartz Direct Impact Technique

Since quartz calibration data above about 30 kbar are of lesser quality, a variation in the above technique is used to obtain higher stress data. An elastic, high impedance material (usually tungsten carbide) is bonded to the front of the quartz gage and is impacted by the specimen. Because of the large difference in impedance of the buffer and the quartz, high

stresses are generated in the specimen and the buffer without exceeding the well-calibrated stress range of th· quartz. Tungsten carbide buffers, for example, reduce the stress induced in the quartz to about one-quarter that in the specimen.

Transmitted Wave

The technique for measuring the profile of a shock wave transmitted through a specimen is shown in Figure 24. An x-cut

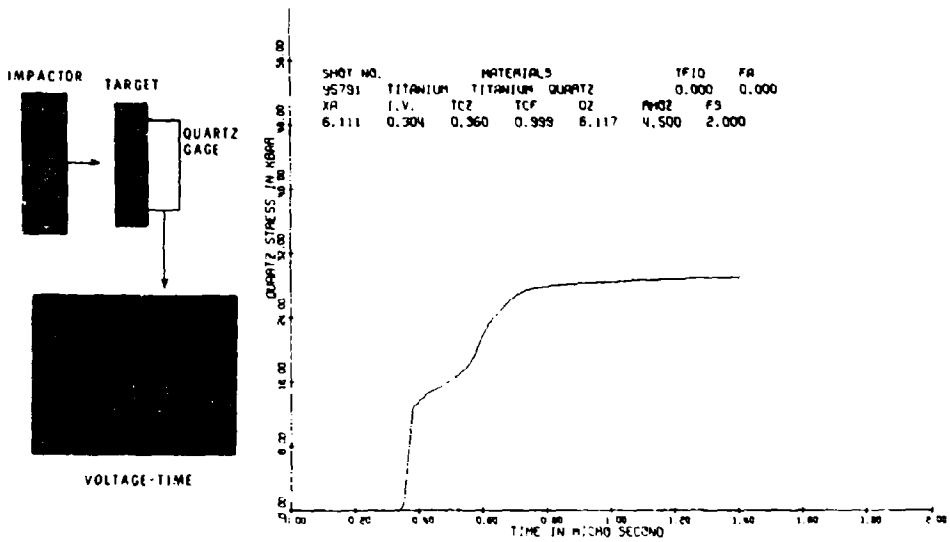

Figure 24 Quartz Transmitted Wave Technique

quartz crystal is placed on the back face of the specimen and the assembly is impacted with an impactor either of the same material as the specimen (where, because of symmetry, $u_p = V_I/2$), or an impactor of different material with known hugoniot. A

stress-wave is generated at impact and propagates through the specimen to the interface with the quartz gage. Here the wave is partially reflected back into the specimen and partially transmitted into the quartz, as determined by stress and particle velocity continuity requirements. Data recording is essentially the same as with direct impact.

Elevated Temperature

For testing at elevated temperatures, the target is radiantly heated by a nichrome-wire heater element placed between the target and the launch tube, as shown in Figure 25. The system is shown both with the heater in position before firing, and retracted for firing (with the target removed to show heater and projectile detail). The target is heated from the front face only to permit instrumentation or optical access to the rear, and temperature is monitored by thermocouple. Heater element voltage is adjusted to bring the target to temperature in ∿10 minutes and the target is allowed to stabilize at test temperature for 5 to 10 minutes.

The target and impactor are aligned at room temperature for planar impact. The target alignment is then monitored during heat-up by an optical-lever system in which a laser beam is reflected off the rear face of the target and displayed, through a series of mirrors, on a screen in the control room. If the target position changes during heating, a remote control system using DC-drive motors allows realignment by rotating the target assembly about either of two axes. Tilt at impact is comparable to that achieved at room temperature.

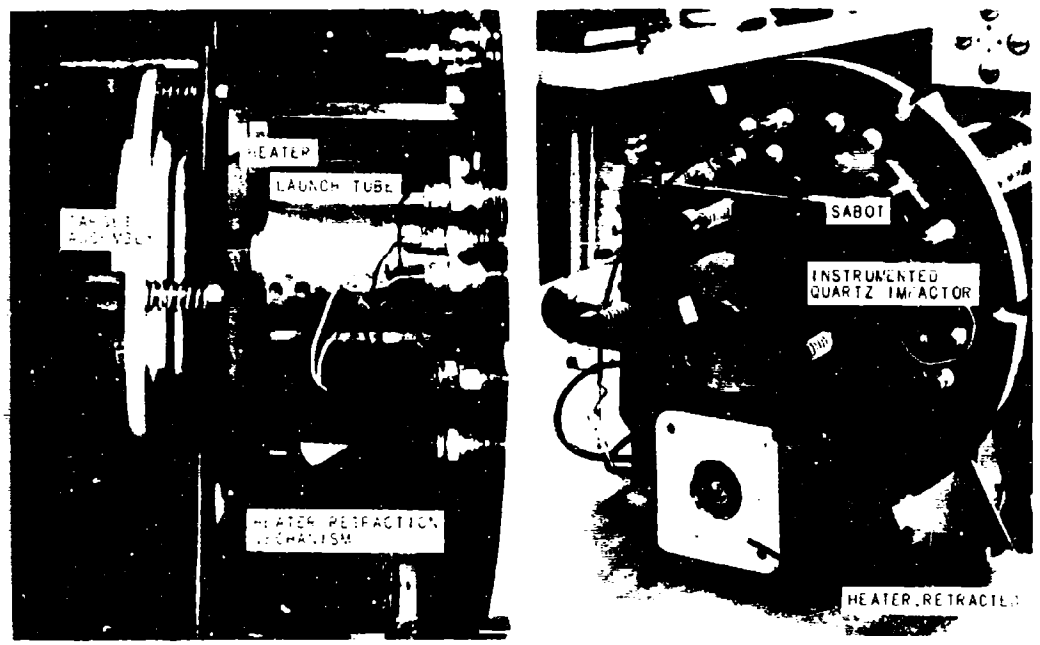

Figure 25 Target Heating System (Target Chamber Removed)

Although designed primarily for quartz gage testing, the heating system can be used with any type of instrumentation, provided the transducer, if any, can withstand exposure to elevated temperature, or the rear surface remains reflective if optical techniques are being used. Velocity interferometer measurements at elevated temperature were easily accomplished with this technique.

Quartz Gage Data Reduction[29]

Two methods are used for determining material stress once the quartz gage current-time record has been converted to quartz stress-time:

A. The end-state or peak-stress level in the quartz is determined as a stress-particle velocity point. Graphical or calculational techniques are then used to solve for the corresponding material stress-particle velocity point. For the direct impact case (Figure 26):

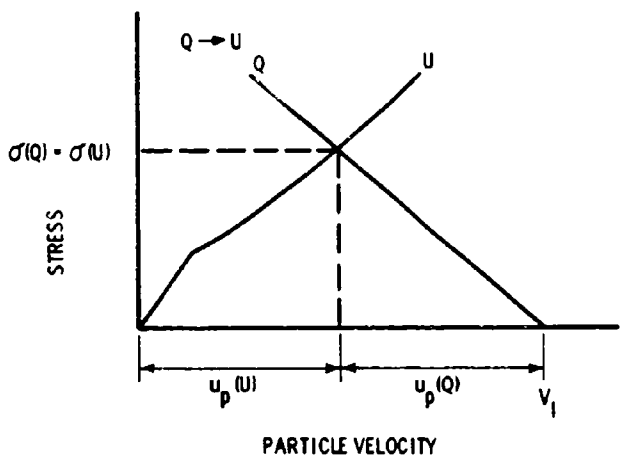

Figure 26 Quartz Direct Impact Analysis

Known - V_I, $\sigma(Q)$

$$U_s(Q) = b_1 + \sqrt{b_2 + b_3\sigma(Q)}\ /b_4$$

$$u_p(Q) = \frac{\sigma(Q)}{\rho_o U_s(Q)}$$

Then - $\sigma(U) = \sigma(Q)$

$$u_p(U) = V_I - u_p(Q)$$

(where b_1, b_2, b_3 and b_4 are constants for x-cut quartz.)

For the direct impact-buffer case (Figure 27):

Known - V_I, $\sigma(Q)$

$$\rho_o C_L(E) = Z$$

$$U_s(Q) = b_1 + \sqrt{b_2 + b_3\sigma(Q)}\ /b_4$$

$$u_p(Q) = \frac{\sigma(Q)}{\rho_o U_s(Q)}$$

Then - $\sigma(U) = \sigma(E) = 1/2(\sigma(Q) + Z \times u_p(Q))$

$$u_p(U) = V_I - \frac{\sigma(E)}{Z}$$

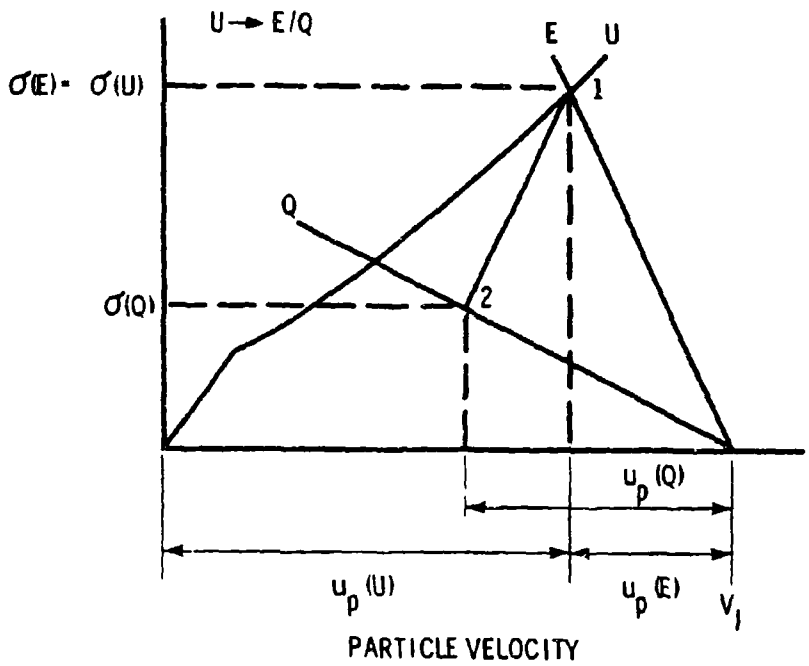

Figure 27 Quartz Direct Impact-Buffer Analysis

For the unknown into unknown transmitted wave case (Figure 28):

Known - V_I, $\sigma(Q)$, $\rho_o(U)$, $C_L(U)$

$$U_s(Q) = b_1 + \sqrt{b_2 + b_3\sigma(Q)}\ /b_4$$

$$u_p(Q) = \sigma(Q)/\rho_o U_s(Q)$$

Then - $u_p(U) = V_I/2$

ELASTIC UNLOADING -

$$\sigma(U) = \rho_o(U)C_L(U)(u_p(Q)-u_p(U))+\sigma(Q)$$

PLASTIC UNLOADING -

$$\sigma(U) = (\sigma(Q)u_p(U))/(2u_p(U) - u_p(Q))$$

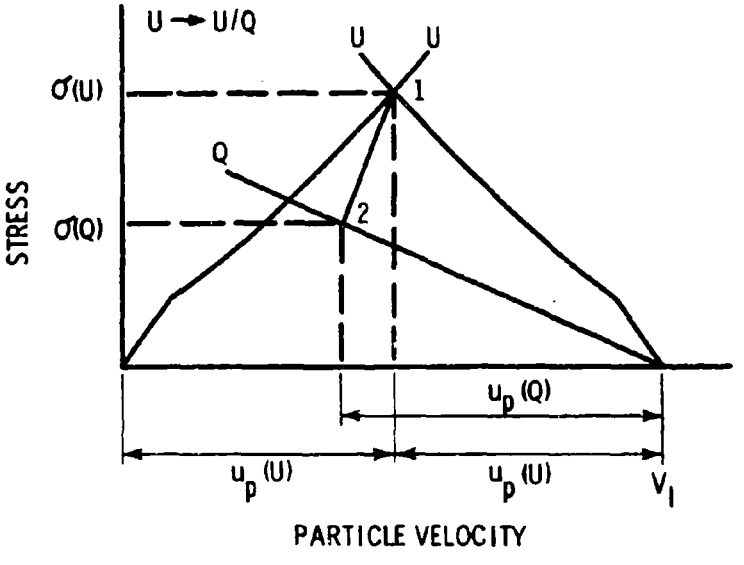

Figure 28 Quartz Transmitted Wave Analysis (Unknown into Unknown/Quartz)

For the known into unknown transmitted wave case (Figure 29):

Known - V_I, $\sigma(Q)$, $\rho_o(U)$, $C_L(U)$

$$U_s(Q) = b_1 + \sqrt{b_2 + b_3\sigma(Q)}\ /b_4$$

$$u_p(Q) = \sigma(Q)/\rho_o U_s(Q)$$

$$\sigma(K) = A + Bu_p(K) + Cu_p^2(K)$$

Then - $\sigma(U) = \sigma(K)$

ELASTIC UNLOADING -

$$Cu_p^2(U) + (\rho_o(U)C_L(U) - B - 2CV_I)u_p(U) + (A + BV_I - \rho_o(U)C_L(U)u_p(Q) - \sigma(Q) + CV_I^2) = 0$$

Solve for $u_p(U)$, two roots.

PLASTIC UNLOADING -

$$\sigma(U) = A + B(V_I - u_p(U)) + C(V_I - u_p(U))^2$$

$$\sigma(U) = \sigma(Q)u_p(U)/(2u_p(U) - u_p(Q))$$

Solve for $u_p(U)$ by iteration.

Elastic unloading is defined as unloading along a line with slope $\rho_o C_L$ for the unknown. Plastic unloading is defined as unloading along a line with slope $\sigma(U)/u_p(U)$. Other unloading paths may be assumed.

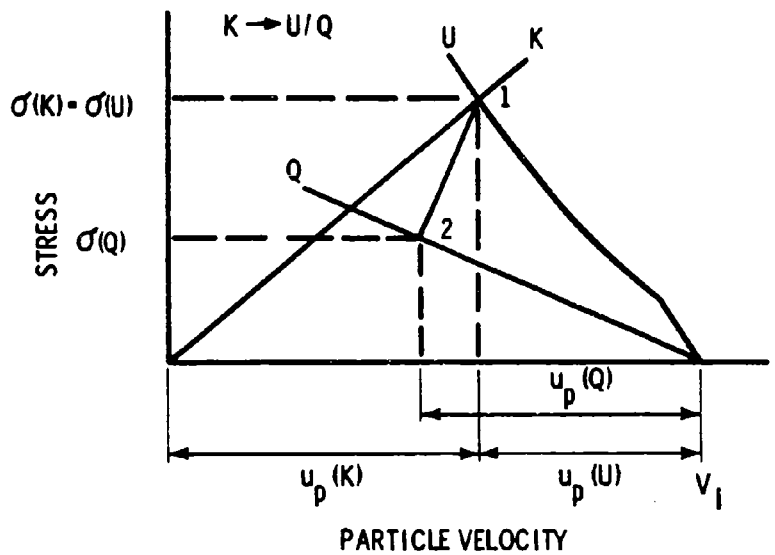

Figure 29 Quartz Transmitted Wave Analysis (Known into Unknown/Quartz)

B. For transmitted wave tests, the stress-time history in the material is deduced from the quartz stress-time by impedance matching. The digitized quartz stress σ_q vs. time data, quartz elastic impedance Z, initial specimen density ρ_o, and thickness X_o, and the initial wave transit time t_o are known. For the first stress increment:

$$\sigma(1) = \sigma_q(1) \frac{Z + Z_o}{2Z}$$

$$u(1) = \sigma(1)/Z_o$$

where $Z_o = \rho_o \frac{X_o}{t_o} = \rho_o D_o$

For subsequent increments (i = 1,2,...):

$$\sigma(i+1) = \sigma(i)+[\sigma_q(i+1)-\sigma_q(i)]\frac{Z + Z(i)}{2Z}$$

$$u(i+1) = u(i) + \frac{\sigma(i+1)-\sigma(i)}{Z(i)}$$

where $Z(i) = \rho(i)\frac{X(i)}{t(i)} = \rho(i)D(i)$

$$X(i) = X(i-1) + \frac{\sigma_q(i)}{Z}[t(i)-t(i-1)]$$

$$\rho(i) = \rho(i-1)\frac{D(i-1)}{D(i-1)-[u(i)-u(i-1)]}$$

The above solution assumes, in addition to the hugoniot jump conditions, no time-dependence and no wave interactions.

Manganin Gage[30]

The manganin gage utilizes the piezoresistive properties of manganin to give stress-time history. The gage has been used from below 1 kbar to over 400 kbar, and can serve as an in-material gage or as an interface stress gage. The gage can be used in a conducting material but the active element must be electrically isolated, making the response time proportional to gage plus insulation thickness. The manganin gage schematic and record from a plexiglas target test is given in Figure 30. The element can be wire or foil in various configurations with resistance ranging from 1 to 50 ohms. A constant-current source is discharged through the gage prior to impact and voltage across the gage is monitored. A stress wave will change the gage resistance, which is recorded as a voltage-time trace. The film record is reduced using the known piezoresistive coefficient of

manganin. As with other "area-averaging" transducers, the effect of tilt should be considered in analyzing the results.

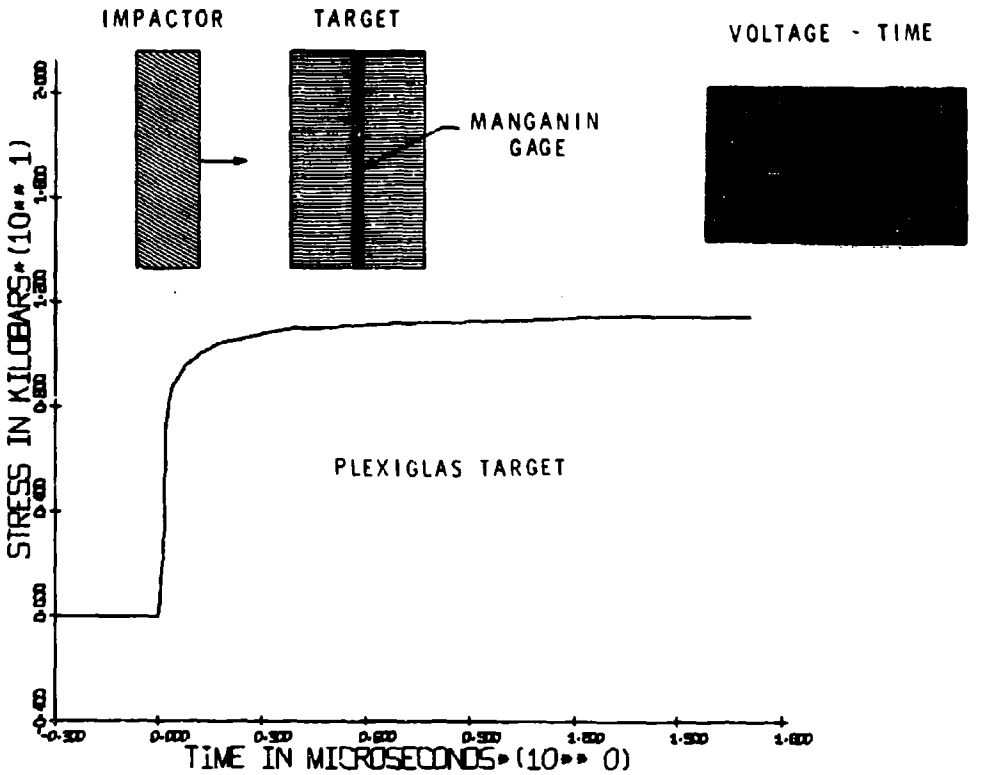

Figure 30 Manganin Gage Technique

Streak Camera Techniques[31]

Streak camera techniques provide equation of state data in the form of shock velocity-particle velocity points, and wave profile data in the form of free surface or interface motion as a function of time. A Beckman and Whitley Model 339B streak camera is used and the three basic applications are for shock arrival measurements (hat target), free surface velocity (shim target), and free surface motion (wedge target).

Hat Target

To measure shock velocity in an impacted specimen, targets are constructed in the form of a two-step cylinder ("hat" configuration) with shock arrival mirrors placed at two levels as shown in Figure 31. (If the surface of the target material can be polished to give good reflectivity, the mirrors can be eliminated.) The impactor and target are of the same material to give $u_p = V_I/2$. At impact a shock is generated and traverses the target to the rear surfaces. The two surfaces are observed through the slit of a streak camera with a xenon flash tube used for lighting. The shock arrival at each level is recorded on film as a change in reflectance. The time required for shock wave travel from the first level to the second is calculated from the film record, knowing the camera sweep rate. This time and the known target dimensions give average shock wave velocity. The film record also provides a measure of shock tilt, which is used for transit time correction. Multiple shock waves can frequently be observed by slight changes in mirror reflectivity as the waves arrive at the two levels.

Shim Target

The shim target technique is used to measure velocity of a shim ($\sim$0.01mm thick), initially weakly bonded to the rear surface of the target, as it crosses a gap of known width as shown in Figure 32. Shims are used rather than the specimen surface itself to insure that if the surface decelerates due to shock attenuation, the shim will continue to move with maximum free surface velocity. The strength of the bond between the shim and target does not measurably influence shim motion. Attenuation targets are constructed with several steps to provide measurements of several propagation distances from one experiment.

Upon arrival of the impact-generated shock wave at the rear surface, the reflectance of the shim surface changes. The shim then crosses the gap and strikes the mirror, giving an abrupt change in mirror reflectance. The gap transit time and the known gap size yield free surface velocity. Shock velocity and shock tilt are also obtained by including data from the side mirrors. Measurements of maximum free surface velocity attained by the specimen surface are accurate to ±2%.

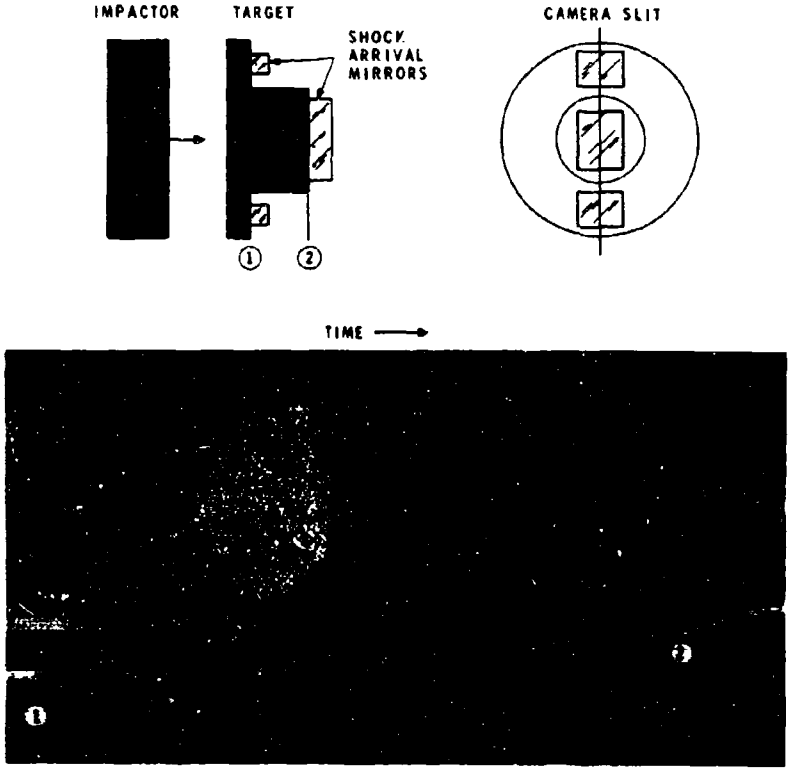

Figure 31 Hat Target Technique

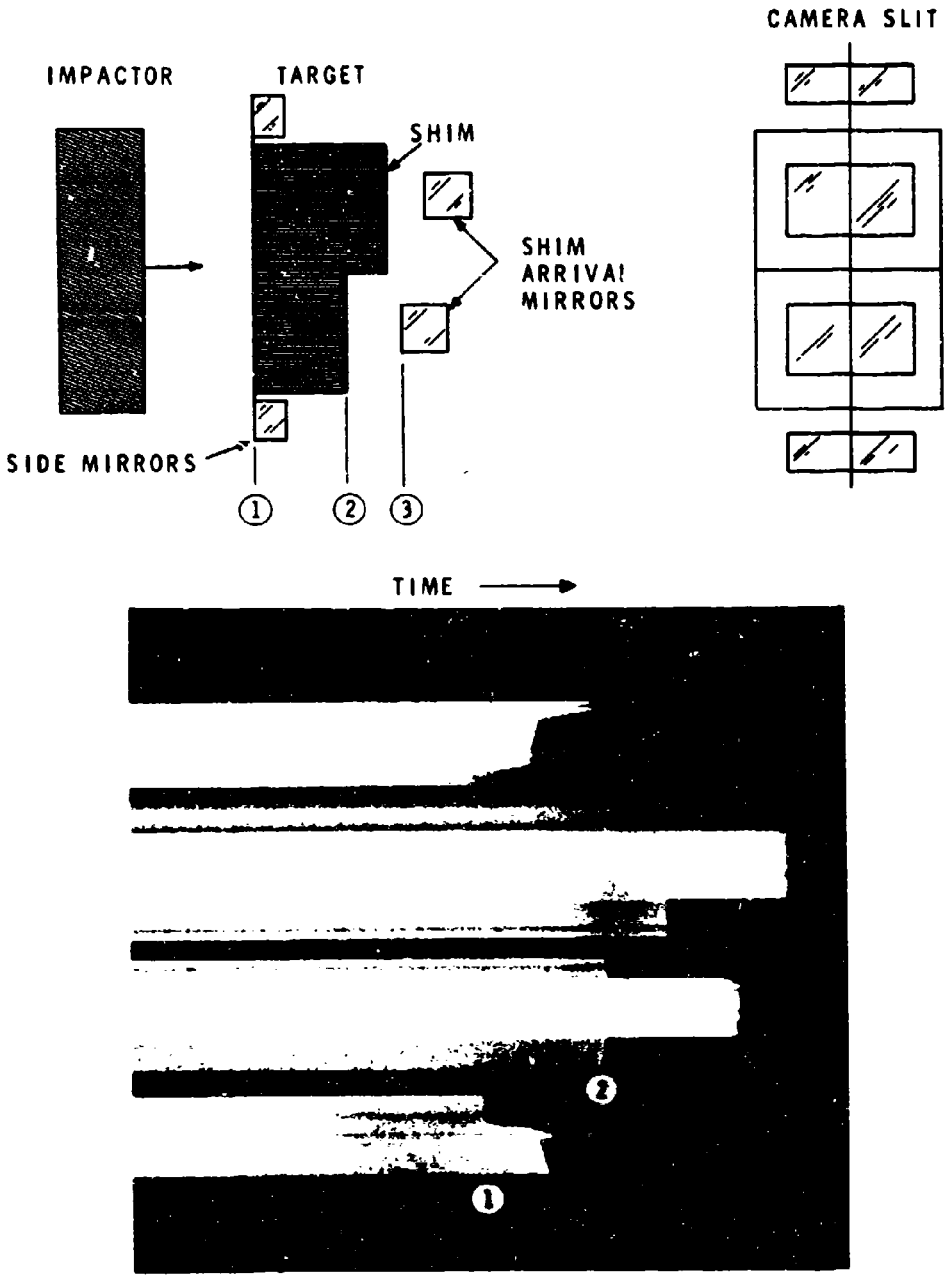

Figure 32 Shim Target Technique

Wedge Target

The wedge target technique illustrated in Figure 33 is used primarily for studying shock wave attenuation. The impactor and target dimensions are selected such that in the thinner

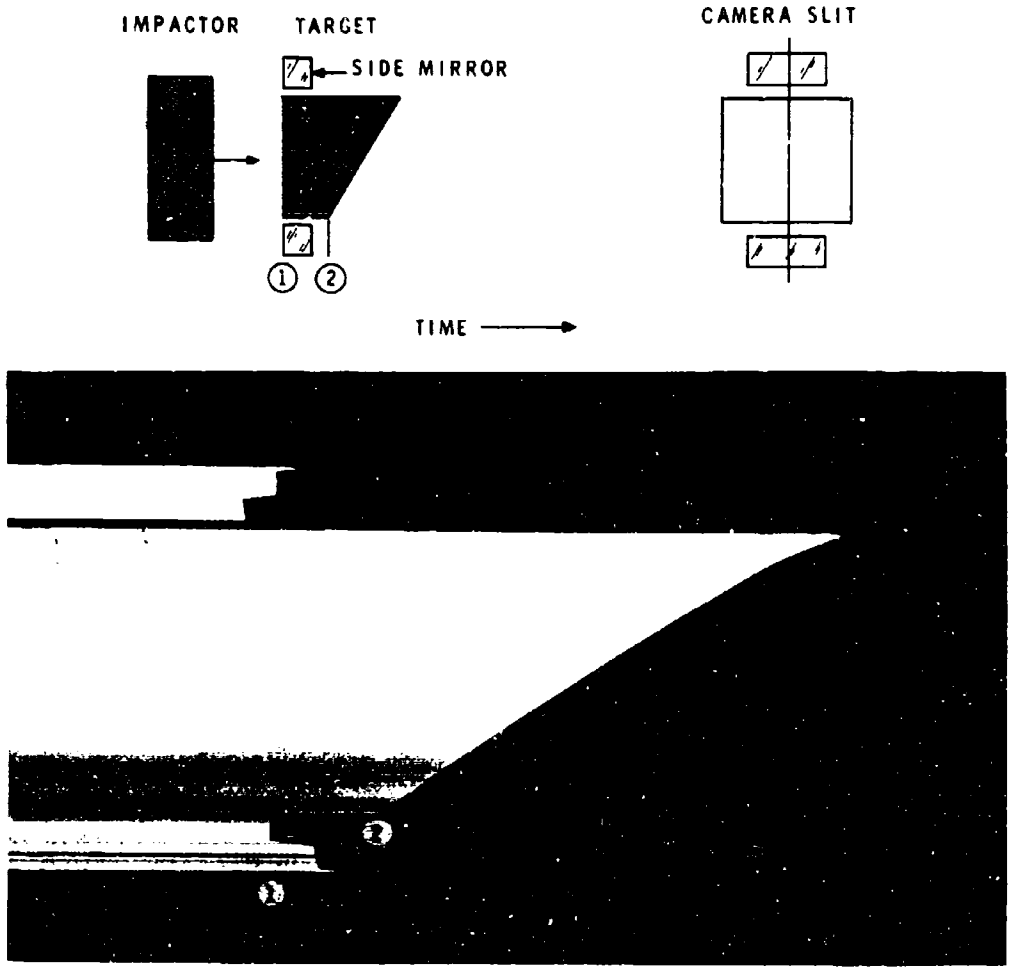

Figure 33 Wedge Target Technique

portion of the wedge the shock wave has not attenuated and constant shock velocity is obtained, while in the thicker part of the wedge the release wave from the rear of the thin impactor has started to attenuate the wave, leading to a decrease in average shock velocity. The shock velocity is proportional to the slope of the streak camera record and the arrival of the release wave and the subsequent attenuation can be deduced from changes in this slope. Tilt data are obtained by use of side mirrors and are used to correct the measured shock velocities. Since the record provides a continuous measure of shock velocity vs. x/x_o rather than discrete x/x_o points as provided by the shim technique, the wedge system is frequently used to measure the exact distance at which the rarefaction wave overtakes the shock wave.

Laser Velocity Interferometer[32]

The laser velocity interferometer measures surface velocity as a function of time. Either free surface motion or motion of the interface between the specimen and a transparent window material can be measured with high spatial and time resolution. A reflective surface is required throughout the recording time, which limits the upper stress level for the technique. The laser velocity interferometer system is shown in Figure 34 with a sample record, and the interferometer details are shown in Figure 35. The system consists of a Perkin-Elmer Model 5800 single-frequency (6328Å) He-Ne laser, a series of mirrors directing the beam to the target, a lens to focus the beam onto the surface being observed, a second series of mirrors to direct the reflected beam to a beam splitter (which sends half the light around an adjustable delay leg), and an IIT Model F4034 photomultiplier (PM) tube with 0.8/nsec rise time and 300 MHz frequency response.

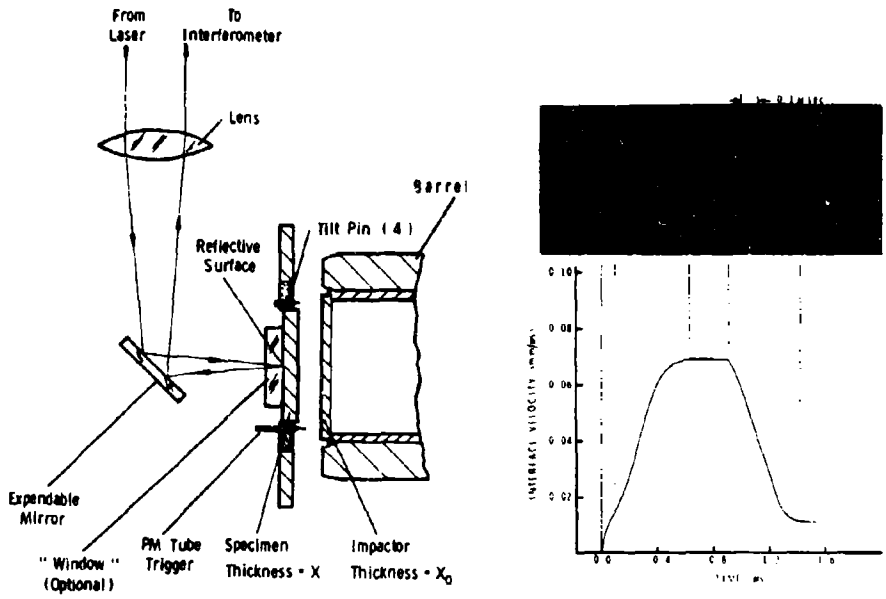

Figure 34 Laser Velocity Interferometer Technique

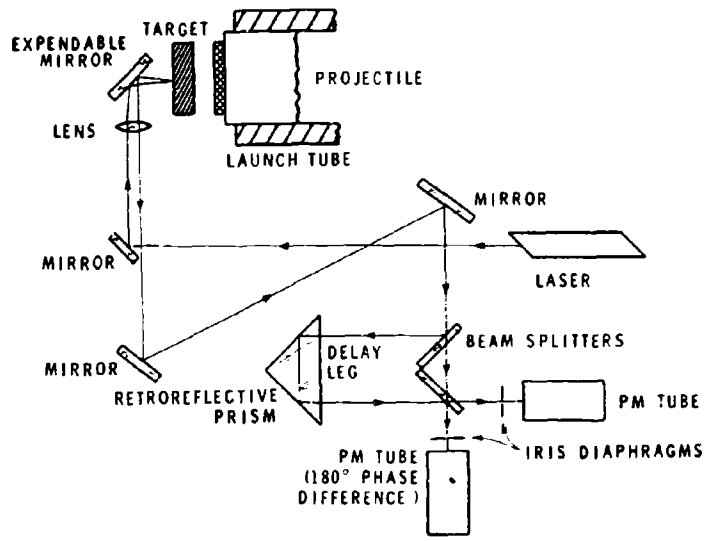

Figure 35 Laser Velocity Interferometer Schematic

A fringe pattern is developed after the two beams recombine at the beam splitter and is focused on the PM tube. The fringe pattern will change as the target surface moves as a result of the doppler shifting of the beam reflected from the moving surface of the specimen. The number of fringes seen by the PM tube per unit time is proportional to the acceleration of the surface.* The proportionality constant or sensitivity of the interferometer is controlled by the delay leg length, i.e., the longer the delay leg, the more fringes obtained for a given change in velocity. The PM tube output goes to Tektronix 519 and 454 oscilloscopes and is recorded on film. The voltage-time trace is reduced to give the velocity-time history of the moving surface, using appropriate interferometer constants (laser wave length, delay leg length, etc.). A projectile and velocity interferometer target are shown in Figure 36. The sabot and target construction are typical for the 102mm compressed gas gun system.

Slanted Resistance Wire[33]

The slanted resistance wire (SRW) technique is used in obtaining distance-time history of the motion of a conducting free surface. The technique can be used over a wide stress range (<1 kbar to >100 kbar) and, since it gives an analog record with good spatial resolution, it can provide data on material anisotropy parallel to the wave front. Operation of the SRW transducer is shown in Figure 37. A thin (12μm) platinum ribbon is placed at a small angle to the rear surface of the specimen,

* It should be noted that for initial motion times less than the delay leg transit time (~5nsec), the system acts as a conventional displacement interferometer.

with one end of the ribbon touching or slightly above the surface, and the other end is held on the order of 0.1mm further from the surface. A constant-current power supply is discharged through the wire just prior to impact. As the rear surface moves under the action of the incident stress wave, the ungrounded length and, therefore, the resistance of the ribbon decreases and is recorded by an oscilloscope as a decrease in voltage. The film record is converted to digital form for data reduction and analysis, including corrections for nonlinearity in voltage vs. distance and for tilt. Velocity-time is then obtained by differentiation of the distance-time record.

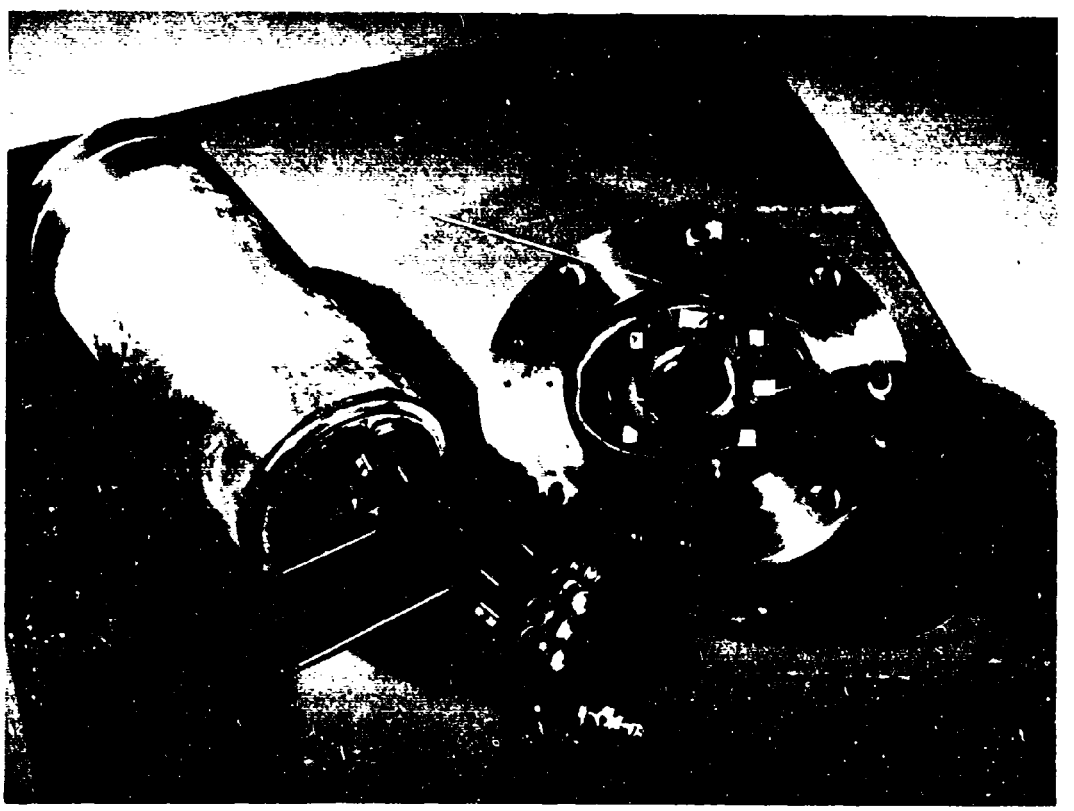

Figure 36 Projectile and Velocity Interferometer Target

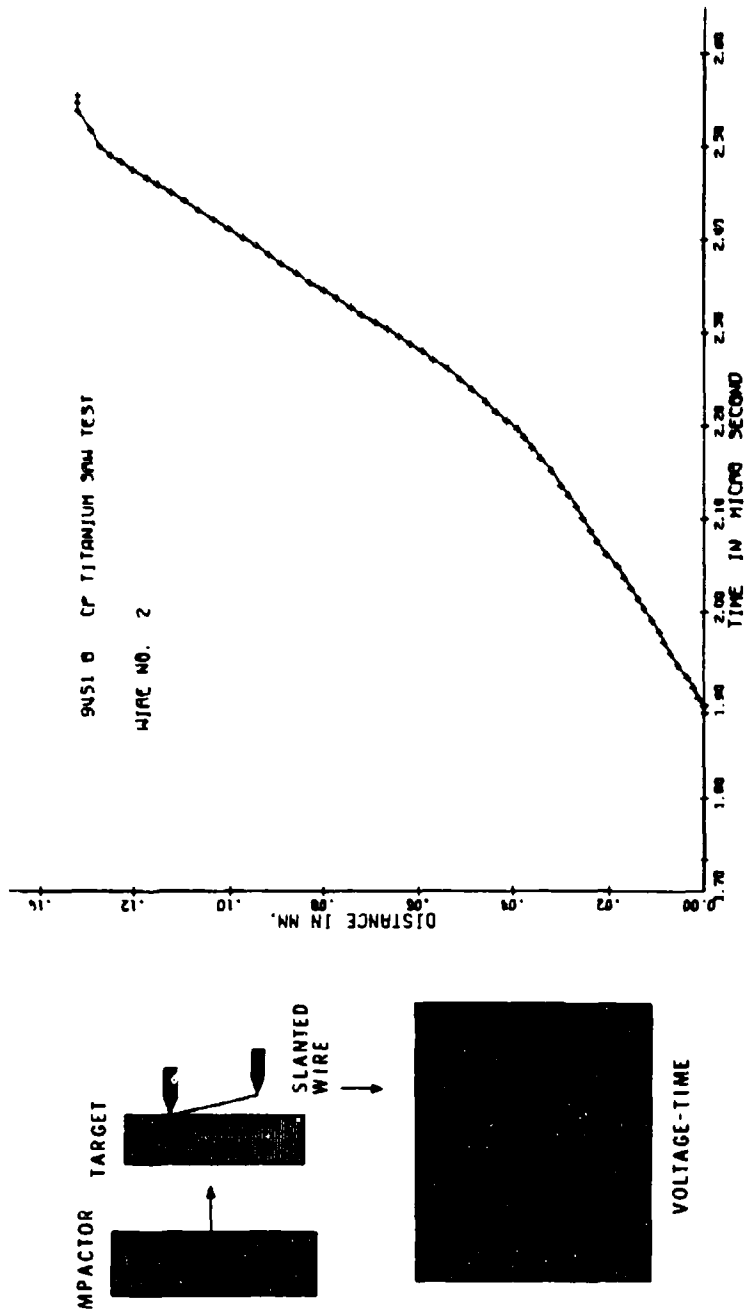

Figure 37 Slanted Resistance Wire Technique

Magnetic Wire Gage[34]

The magnetic wire gage provides a direct measure of particle velocity in a nonconducting material as a function of time. The range of velocities over which the gage can be used is essentially limited only by the noise level and response time of the electronics used to monitor the gage, provided gage integrity is maintained. The gage is normally used in the "sandwich" configuration, with rise-time proportional to gage thickness. The technique is shown schematically in Figure 38 with a representative record from a fused quartz target (which has a dispersive or ramped compressive wave). A thin (~10μm) copper foil is placed in the target, which is then placed in a magnetic field such that motion of the wire will cut the lines of force. A stress wave in the target will cause the wire to move at the material particle velocity, giving an induced voltage of:

$$V = B \times u_p \times d$$

where B is magnetic flux density, u_p is particle velocity, and d is gage length. Typical values of B and d are 1000 gauss and 6 mm, respectively.

The induced voltage is recorded by an oscilloscope, and the film record is reduced to give a particle velocity-time history. Since the gage measures over a length, the data must be corrected for shock wave tilt.

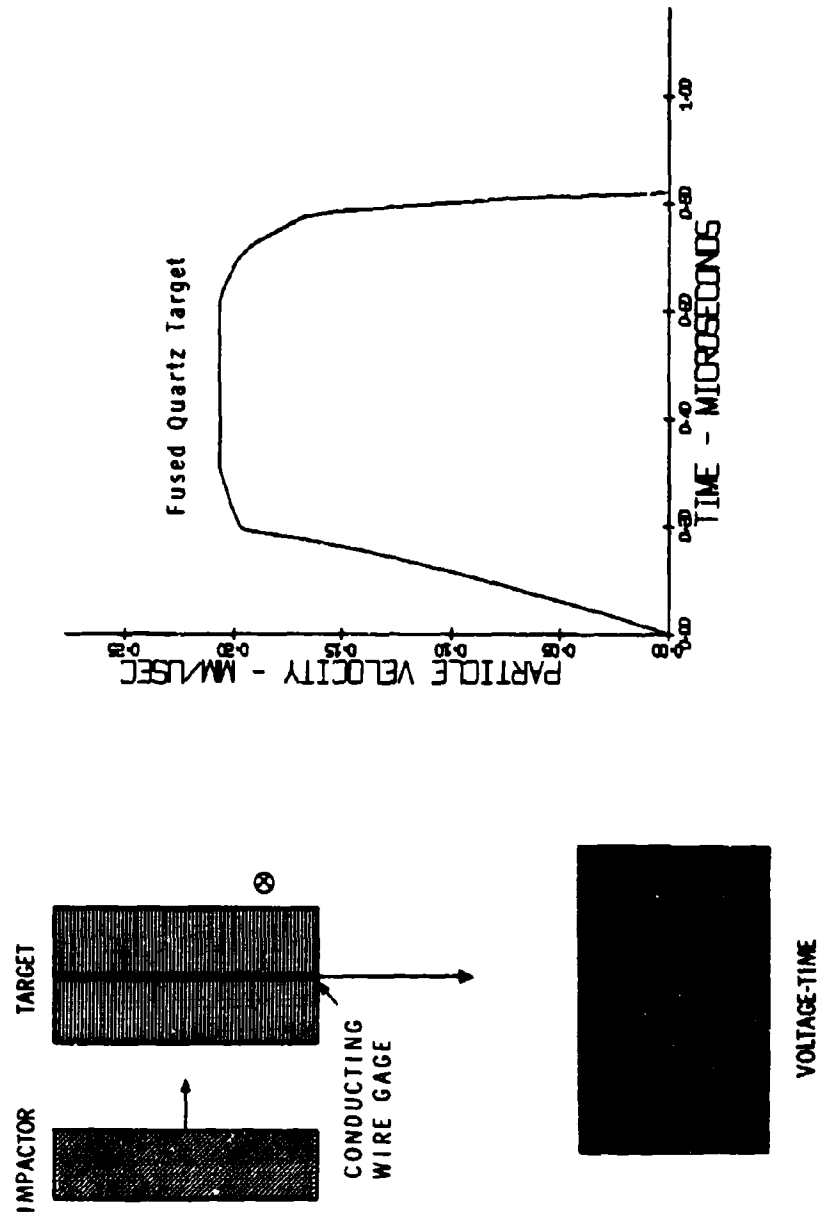

Figure 38 Magnetic Wire Technique

SECTION IV

SPALL TESTS

Spall fracture by plate impact results from reflection of compressive stress pulses from a relatively low impedance interface (normally a free surface) and their subsequent interaction. Spall fracture studies can be carried out using both active and passive techniques. Active techniques provide quantitative, time-resolved data on the influence of internal fractures or spall surfaces on shock wave profiles.[35] The primary instrumentation used is the laser velocity interferometer which provides a time-history of surface motion. The relation between rear surface motion and spall plane growth is shown in Figure 39 and representative results from a spall test are given in Figure 40. Passive techniques involve the recovery and examination of shock-loaded specimens. Subsequent metallographic examination establishes the type and degree of damage, which can be correlated with impact parameters such as velocity, impactor thickness and target thickness.

RECOVERY TESTS[26,36,37]

The spall behavior of metals is generally studied by carrying out a series of impact and recovery tests, where the target specimen is sectioned across a diameter, polished, etched and examined optically at a magnification of 50 to 100X. The specimen is then graded or classified according to the degree of fracture that has occurred, which can range from no observable

fractures to complete material separation. The incipient spall threshold is defined as the impact velocity (for a given set of test parameters) corresponding to the onset of microfracture. One could also establish a complete fracture or separation threshold, but this is not recommended as a primary spall criterion since it is more likely to be influenced by edge effects (loss of one-dimensional strain conditions) and by recovery-induced damage.

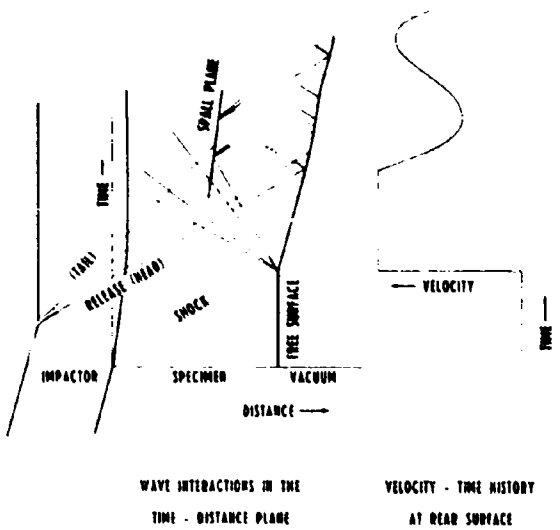

Figure 39 Wave Interaction in Spall Test

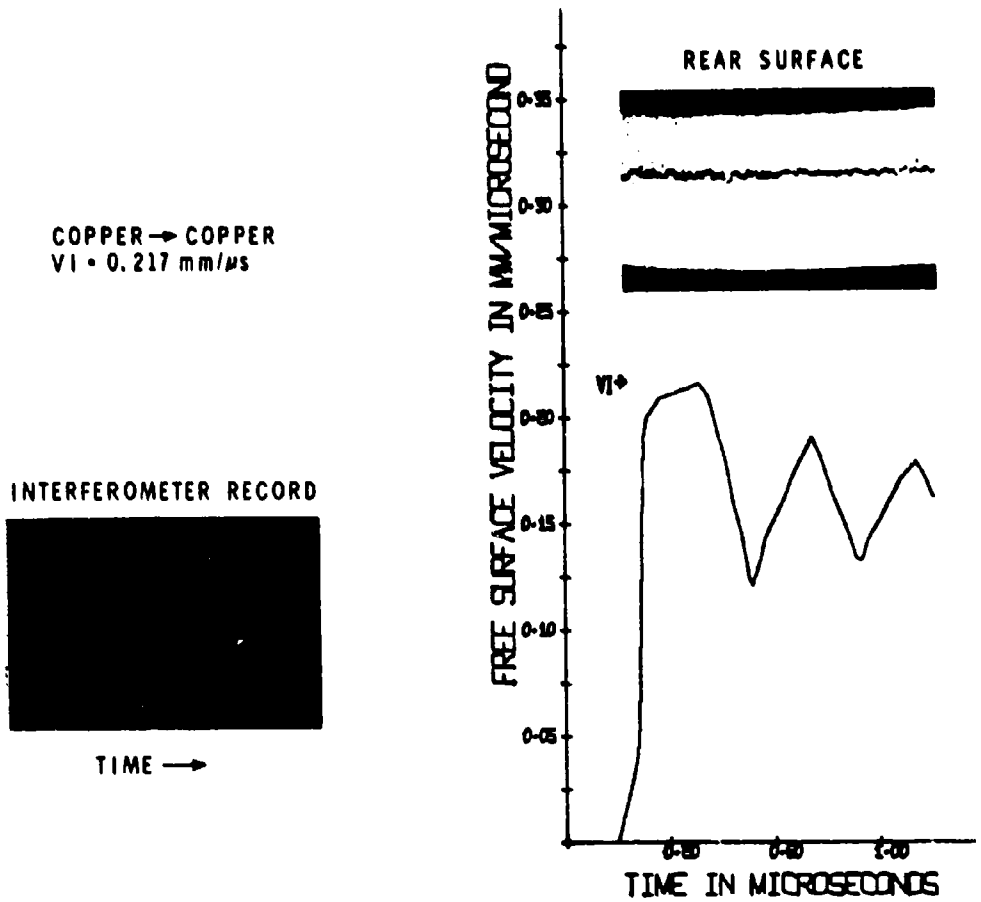

Figure 40 Velocity Interferometer Spall Test Results

Room Temperature Testing

Spall recovery tests are conducted on the 63.5mm compressed-gas gun. The room temperature test setup is shown in Figure 41. The impactor is bonded to a plastic sabot with epoxy resin. The back of the sabot is closed with a plastic disc, and the sabot is vented to allow pressure equalization when the barrel is evacuated. The target is mounted in a urethane alignment

ring and placed in the mouth of the sabot stripper. To position the target, the sabot assembly is forced against the target until it slips, bringing the impactor and target into alignment. Verification of this scheme with the alignment fixture described below indicates that the two methods are comparable. Non-planarity of impact of approximately 10^{-3} radians is maintained, sufficient to regard tilt as unimportant in the interpretation of results. The front lip of the sabot stripper is slightly smaller in diameter than the sabot shell, but larger than the target diameter. This allows the target and impactor to enter the recovery area within the tube but prevents any pieces of the sabot shell from entering and causing post-impact damage. The recovery tube is filled with an energy-absorbing material.

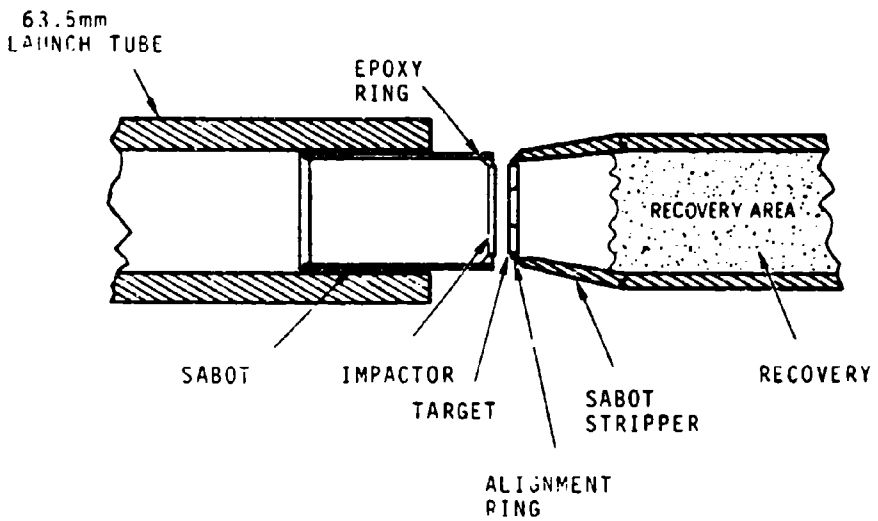

Figure 41 Room Temperature Spall Test Schematic

Elevated Temperature Testing

Elevated temperature spall tests utilize the furnace shown in Figure 42 (with one heater element removed for clarity), which provides radiant heating in the vacuum environment of the target chamber. The heating elements are spiral wound resistance wires mounted in retractable doors. The targets are supported in the furnace on four ceramic pins and are heated uniformly from both sides. The specimen temperature is monitored at the nominal spall plane near the periphery, and the thermocouple output is recorded on a strip chart recorder. The voltage to the heating elements is adjusted to bring the target to test temperature in approximately 10 minutes and the target is then allowed to stabilize at this temperature for an additional 5 to 10 minutes.

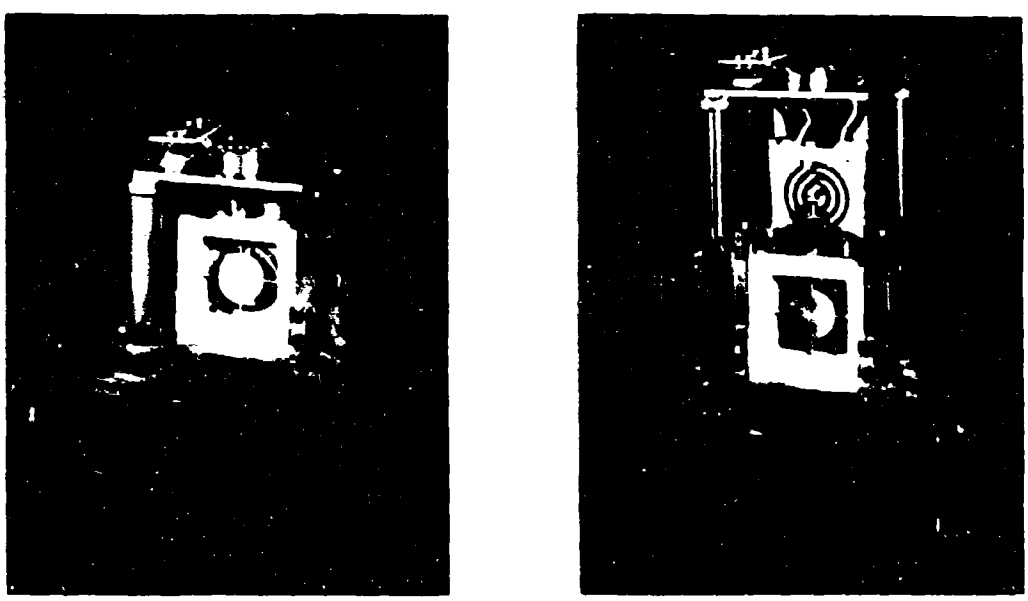

Figure 42 Spall Test Furnace (One Door Removed)

Caution should be exercised in the choice of heating and stabilization times. Studies of several materials heated in times from milliseconds to hundreds of hours have shown marked decreases in yield strength occurring on the order of minutes, due to diffusion mechanisms.[38] Misleading results can be obtained if tests are conducted after softening has occurred, especially if results are to be correlated with tests made in the sub-microsecond heating times arising from energy deposition.

Alignment of the impactor and target is made using an electrical fixture with three pins equally spaced on a 32mm diameter circle, each pin consisting of two hardened steel dowels with a piece of 1-mil mylar between them for electrical insulation. The outer ends of each pin are radiused and their lengths have been adjusted to define planes parallel within ±2μm. Each pin segment is connected to an indicating light through a high impedance circuit which prevents arcing and heating between the contact point and the target. The actual alignment is accomplished by inserting the fixture between the target and impactor, with a slight pressure applied to the rear of the sabot. The furnace, which is mounted on a spherical bearing and is free to move with two degrees of freedom (sufficient to fix a plane in space), is then moved with micrometer screws until all six indicating lights (three for the impactor and three for the target) are lit.

METALLOGRAPHIC EXAMINATION

Conventional light microscopy is the most common way of examining recovered spall specimens. A Zeiss Ultraphot II research metallograph is used which provides 8 to 2500X magnification,

with bright field, dark field, polarized or phase contrast illumination. A typical series of photomicrographs obtained for aluminum is shown in Figure 43. The level of damage for each impact velocity is indicated by the symbols at the left of each picture. These symbols are defined as follows:

- ● Complete Separation
- ◒ Above Incipient
- ◙ Incipient Spall
- ◒ Below Incipient
- O No Cracks at 50X

Scanning electron microscopy is used in the study of spall fractures and fracture surfaces. A Joelco Model JSM-U3 microscope with 20 to 10^5X magnification provides much greater depth of field and resolution than is possible with optical microscopy, and permits detailed examination of fracture surfaces.

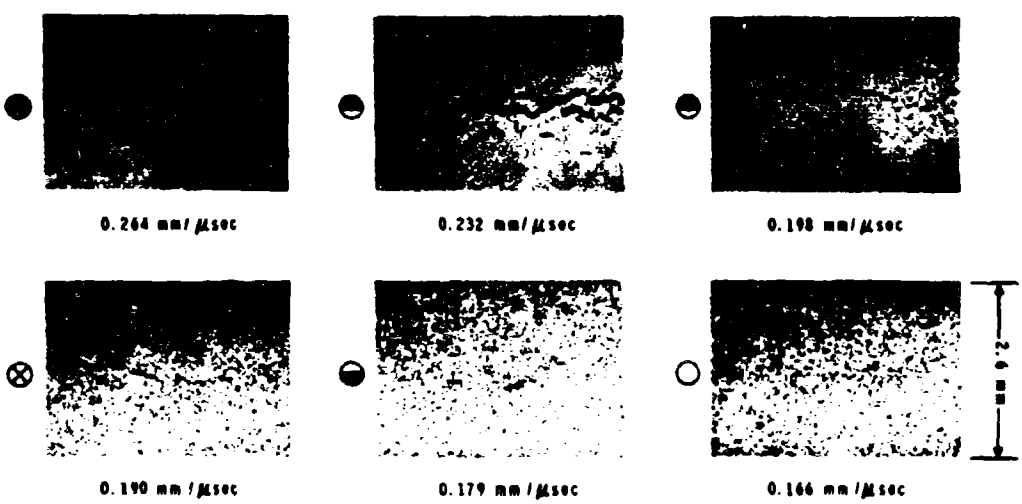

Figure 43 Spall Fractures in 6061-T6 Aluminum, Optical Micrographs

SEM micrographs of sectioned spall specimen (similar to those in Figure 43) are shown in Figure 44, and micrographs of fracture surfaces from completely separated specimens are shown in Figure 45.

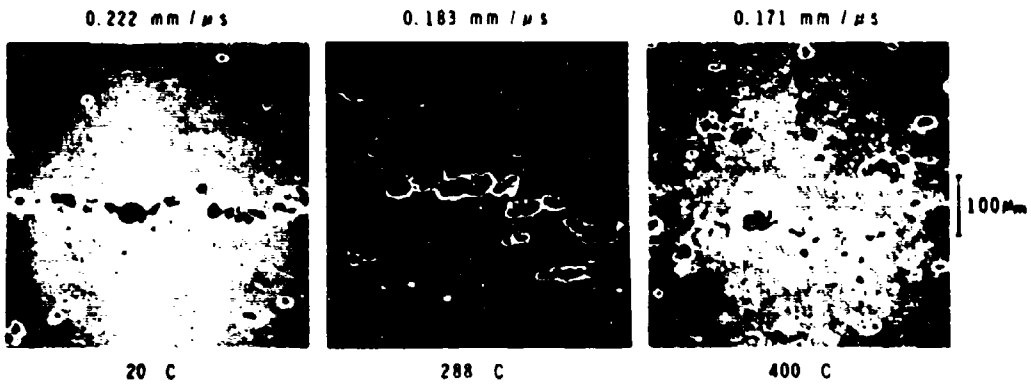

Figure 44 Spall Fractures in 6061-T6 Aluminum, Scanning Electron Micrographs

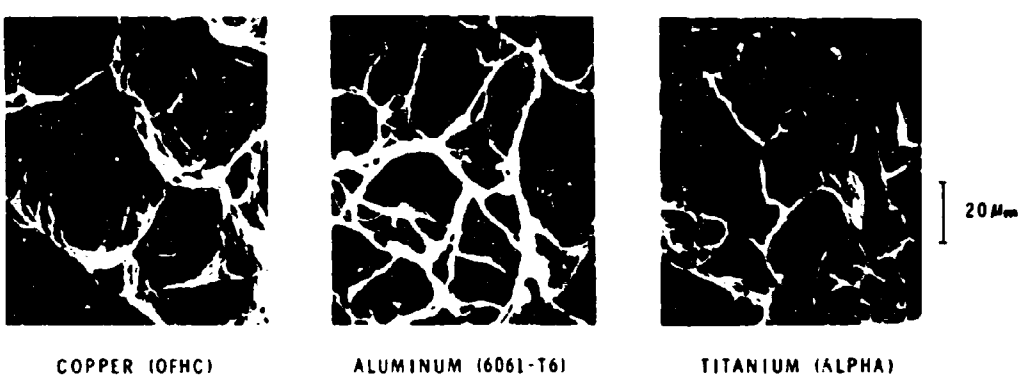

Figure 45 Spall Fracture Surfaces, Scanning Electron Micrographs

REFERENCES

1. Isbell, W. M., Christman, D. R., Babcock, S. G., Michaels, T. E. and Green, S. J., "Measurements of Dynamic Properties of Materials, Vol. I: Summary of Results", DASA-2501-1, Manufacturing Development, Materials and Structures Laboratory, General Motors Corporation, (AD712847), 1970.

2. Christman, D. R., Isbell, W. M., Babcock, S. G., McMillan, A. R. and Green, S. J., "Measurements of Dyanmic Properties of Materials, Vol. III: 6061-T6 Aluminum", DASA-2501-3, Manufacturing Development, Materials and Structures Laboratory, General Motors Corporation, 1971.

3. Christman, D. R., Michaels, T. E., Isbell, W. M. and Babcock, S. G., "Measurements of Dynamic Properties of Materials, Vol. IV: Alpha Titanium", DASA-2501-4, Manufacturing Development, Materials and Structures Laboratory, General Motors Corporation, 1971.

4. Christman, D. R., Isbell, W. M. and Babcock, S. G., "Measurements of Dynamic Properties of Materials, Vol. V: OFHC Copper", DASA-2501-5, Manufacturing Development, Materials and Structures Laboratory, General Motors Corporation, 1971.

5. Isbell, W. M., Christman, D. R. and Babcock, S. G., Measurements of Dynamic Properties of Materials, Vol. VI: Tantalum", DASA-2501-6, Manufacturing Development, Materials and Structures Laboratory, General Motors Corporation, 1971.

6. Clark, D. S. and Wood, D. S., "The Time Delay for the Initiation of Plastic Deformation at Rapidly Applied Constant Stress", ASTM Proc., Vol. 49, p. 717-737, 1949.

7. Campbell, J. D. and Marsh, K. J., "The Effect of Grain Size on the Delayed Yielding of Mild Steel", Phil. Mag., Vol. 7, p. 933-952, 1962.

8. Maiden, C. J. and Green, S. J., "Compressive Strain-Rate Tests on Six Selected Materials at Strain Rates from 10^{-3} to 10^{4} In/In/Sec", ASME Trans. - J. Appl. Mech., Ser. E, Vol. 33, p. 496-504, 1966.

9. Kolsky, H., "An Investigation of the Mechanical Properties of Materials at Very High Rates of Loading", Phys. Soc. Proc. B, Vol. 62, p. 676-700, 1949.

10. Davies, E. D. H. and Hunter, S. C., "The Dynamic Compression Testing of Solids by the Method of the Split Hopkinson Bar", J. Mech. Phys. Solids, Vol. 11, p. 155-179, 1963.

11. Babcock, S. G. and Perkins, R. D., "High Strain-Rate Response of Three Heat-Shield Materials at Elevated Temperatures", SAMSO-TR-68-71, Vol. II, Manufacturing Development, Materials and Structures Laboratory, General Motors Corporation, (AD842604L), 1968.

12. Green, S. J., Leasia, J. D., Perkins, R. D. and Maiden, C. J., "Development of Multiaxial Stress High Strain-Rate Techniques", SAMSO-TR-68-71, Vol. III, Manufacturing Development, Materials and Structures Laboratory, General Motors Corporation, (AD847163L), 1968.

13. Perkins, R. D., Jones, A. H., Green, S. J. and Leasia, J. D., "Multiaxial Loading Behavior of Four Materials Including ATJ-S Graphite and RAD-6300 Carbon Phenolic", SAMSO-TR-69-393, Vol. I, Manufacturing Development, Materials and Structures Laboratory, General Motors Corporation, (AD874866L), 1969.

14. Perkins, R. D., Jones, A. H. and Green, S. J., "Determination of Multiaxial Stress Behavior of Solenhofen Limestone and Westerly Granite", DASA-2438, Manufacturing Development, Materials and Structures Laboratory, General Motors Corporation, 1970.

15. Schierloh, F. L., Chaney, R. D. and Green, S. J., "An Application of Acquisition and Reduction of Data of Variable Short Time Tests", Exp. Mech., Vol. 10, p. 23N-28N, 1970.

16. Babcock, S. G., Hochstein, P. A. and Jacobs, L. J., "High Heating Rate Response of Two Materials from 72 to 6000°F", SAMSO-TR-69-393, Vol. II, Manufacturing Development, Materials and Structures Laboratory, General Motors Corporation, (AD867427L), 1969.

17. Babcock, S. G. and Hochstein, P. A., "High Strain-Rate Testing of Rapidly Heating Conductive Materials to 7000°F", Exp. Mech., Vol. 10, p. 78-83, 1970.

18. McSkimin, H. J., "Pulse Superposition Method for Measuring Ultrasonic Wave Velocities in Solids", Acoust. Soc. Am. J., Vol. 33, p. 12-16, 1961.

19. Lingle, R., Havens, J. R. and Jones, A. H., "Ultrasonic Velocity Measurements in Nodular Iron Castings", MSL-69-49, Manufacturing Development, Materials and Structures Laboratory, General Motors Corporation, 1969.

20. Mattaboni, P. and Schreiber, E., "Method of Pulse Transmission Measurements for Determining Sound Velocities", J. Geophys. Res., Vol. 72, p. 5160-5163, 1967.

21. McSkimin, H. and Andreatch, P., "Analysis of Pulse Superposition Method for Measuring Ultrasonic Wave Velocities as a Function of Temperature and Pressure", Acoust. Soc. Am. J., Vol. 34, p. 609-615, 1962.

22. Asay, J. R., Lamberson, D. L. and Guenther, A. H., "Pressure and Temperature Dependence of the Acoustic Velocities in Polymethylmethacrylate", J. Appl. Phys., Vol. 40, p. 1768-1783, 1969.

23. Kolsky, H., Stress Waves in Solids, S1098, Dover Publications, Inc., New York, 1963.

24. Mason, W. P., "Acoustic Properties of Solids", American Institute of Physics Handbook, 2nd. Ed., p. 3-28 - 3-97, 1963.

25. Barsch, G. R. and Chang, Z. P., "Adiabatic, Isothermal, and Intermediate Pressure Derivatives of the Elastic Constants for Cubic Symmetry", Phys. Stat. Sol., Vol. 19, p. 129-151, 1967.

26. Christman, D. R., Froula, N. H. and Babcock, S. G., "Dynamic Properties of Three Materials, Vol. I: Beryllium", MSL-68-33, Vol. I, Manufacturing Development, Materials and Structures Laboratory, General Motors Corporation, 1968.

27. Isbell, W. M., Shipman, F. H. and Jones, A. H., "Hugoniot Equation of State Measurements for Eleven Materials to Five Megabars", MSL-68-13, Manufacturing Development, Materials and Structures Laboratory, General Motors Corporation, (AD721920), 1968.

28. Ingram, G. E. and Graham, R. A., "Quartz Gauge Technique for Impact Experiments", SC-DC-70-4932, Sandia Laboratories, 1970.

29. Chin, H. C., "QZ: A Computer Program to Analyze X-Cut Quartz Data Obtained from Shock Loading", MSL-70-15, Manufacturing Development, Materials and Structures Laboratory, General Motors Corporation, 1970.

30. Keough, D. D., "Procedure for Fabrication and Operation of Manganin Shock Pressure Gages", AFWL-TR-68-57, Stanford Research Institute, (AD839983), 1968.

31. McMillan, A. R., Isbell, W. M. and Jones, A. H., "High Pressure Shock Wave Attenuation", DASA-2425, Manufacturing Development, Materials and Structures Laboratory, General Motors Corporation, 1971.

32. Barker, L. M., "Fine Structure of Compressive and Release Wave Shapes in Aluminum Measured by the Velocity Interferometer Technique", Behavior of Dense Media under High Dynamic Pressures, Gordon and Breach, New York, p. 483-505, 1968.

33. Barker, L. M. and Hollenbach, R. E., "System for Measuring the Dynamic Properties of Materials", Rev. Sci. Instr., Vol. 35, p. 742-746, 1964.

34. Dremin, A. N. and Adadurov, G. A., "The Behavior of Glass Under Dynamic Loading", Sov. Phys. Solid State, Vol. 6, p. 1379-1384, 1964.

35. Isbell, W. M. and Christman, D. R., "Shock Propagation and Fracture in 6061-T6 Aluminum from Wave Profile Measurements", DASA-2419, Manufacturing Development, Materials and Structures Laboratory, General Motors Corporation, (AD705536), 1970.

36. Lundergan, C. D., "Spall Fracture", AST-TDR-63-140, Proc. Symposium on Structural Dynamics Under High Impulse Loading, p. 357-381, (AD408777), May, 1963; also, Sandia Corporation Report SCDC-2845.

37. Warnica, R. L., "Spallation Thresholds of S-200 Beryllium, ATJ-S Graphite and Isotropic Boron Nitride at 75°F, 500°F and 1000°F", MSL-68-18, Manufacturing Development, Materials and Structures Laboratory, General Motors Corporation, 1968.

38. Babcock, S. G., Langan, J. J., Norvey, D. B., Michaels, T. E. and Schierloh, F. L., "Characterization of Three Aluminum Alloys", AMMRC-CR-71-3, Manufacturing Development, Materials and Structures Laboratory, General Motors Corporation, 1971.